Monteiro, F. M., Pancost, R. D., Ridgwell, A. J., & Donnadieu, Y. (2012). Nutrients as the dominant control on the spread of anoxia and euxinia across the Cenomanian-Turonian oceanic anoxic event (OAE2): Model-data comparison. Paleoceanography, 27(4), [PA4209]. 10.1029/2012PA002351

# Nutrients as the dominant control on the spread of anoxia and euxinia across the Cenomanian-Turonian oceanic anoxic event (OAE2): Model-data comparison

F. M. Monteiro,[1] R. D. Pancost,[2] A. Ridgwell,[1] and Y. Donnadieu[3]

Received 1 June 2012; revised 19 October 2012; accepted 24 October 2012; published 15 December 2012.

[1] The Cenomanian-Turonian oceanic anoxic event (OAE2) is characterized by large perturbations in the oxygen and sulfur cycles of the ocean, potentially resulting from changes in oxygen supply (via oxygen solubility and ocean circulation) and in marine productivity. We assess the relative impact of these mechanisms, comparing model experiments with a new compilation of observations for seafloor dysoxia/anoxia and photic zone euxinia. The model employed is an intermediate-complexity Earth system model which accounts for the main ocean dynamics and biogeochemistry of the Cretaceous climate. The impact of higher temperature and marine productivity is evaluated in the model as a result of higher atmospheric carbon dioxide and oceanic nutrient concentrations. The model shows that temperature is not alone able to reproduce the observed patterns of oceanic redox changes associated with OAE2. Observations are reproduced in the model mainly via enhanced marine productivity due to higher nutrient content (responsible for 85% of the change). Higher phosphate content could have been sustained by increased chemical weathering and phosphorus regeneration from anoxic sediments, which in turn induced an enhanced nitrogen nutrient content of the ocean via nitrogen fixation. The model also shows that the presence of seafloor anoxia, as suggested by black-shale deposition in the proto-North Atlantic Ocean before the event, might be the result of the silled shape and lack of deep-water formation of this basin at the Late Cretaceous. Overall our model-data comparison shows that OAE2 anoxia was quasi-global spreading from 5% of the ocean volume before the event to at least 50% during OAE2.

**Citation:** Monteiro, F. M., R. D. Pancost, A. Ridgwell, and Y. Donnadieu (2012), Nutrients as the dominant control on the spread of anoxia and euxinia across the Cenomanian-Turonian oceanic anoxic event (OAE2): Model-data comparison, *Paleoceanography*, *27*, PA4209, doi:10.1029/2012PA002351.

## 1. Introduction

[2] Oceanic anoxic events (OAEs) are severe ocean biogeochemical events common to the Cretaceous period [*Schlanger and Jenkyns*, 1976; *Schlanger et al.*, 1987; *Leckie et al.*, 2002; *Jenkyns*, 2010]. These events are characterized by widespread marine deposition of laminated organic carbon-rich layers (black shales), indicating dysoxic if not anoxic conditions at the seafloor [*Arthur and Sageman*, 1994]. OAEs are associated with positive carbon isotope excursions (CIE) recorded in both marine and continental sedimentary archives suggesting strong perturbations of the global carbon cycle [*Hasegawa*, 1997; *Weissert et al.*, 1998; *Jenkyns*, 2003, 2010]. Other common features of the OAEs include sea level rise [*Erbacher et al.*, 1996; *Voigt et al.*, 2006] and changes in stratification and mixing [*Wilson and Norris*, 2001; *Erbacher et al.*, 2001; *Watkins et al.*, 2005]. Changes in marine productivity and major turnovers in the marine biota are also common [*Jarvis et al.*, 1988; *Erbacher and Thurow*, 1997; *Kuypers et al.*, 2002; *Erba*, 2004; *Browning and Watkins*, 2008]. Two of the Cretaceous OAEs are particularly identified as significant globally, OAE1a in the early Aptian (120 Myrs), and OAE2 at the Cenomanian-Turonian boundary (93.5 Myrs). We focus here on OAE2.

[3] Usually associated with the plateau of maximum carbon isotope excursion [*Kuypers et al.*, 2002; *Tsikos et al.*, 2004; *Erbacher et al.*, 2005], OAE2 is estimated to last about 250 to 700 kyrs [*Kolonic*, 2005; *Sageman et al.*, 2006; *Kuroda et al.*, 2007]. Seafloor dysoxia/anoxia, already established in the proto-North Atlantic Ocean before OAE2, spread to most of the Atlantic and Indian Oceans, Southwest Tethys Sea and possibly in the equatorial Pacific Ocean during the event [*Schlanger et al.*, 1987; *Sinninghe Damsté*

[1]School of Geographical Sciences, University of Bristol, Bristol, UK.
[2]Organic Geochemistry Unit, Bristol Biogeochemistry Research Centre and The Cabot Institute, School of Chemistry, University of Bristol, Bristol, UK.
[3]Laboratoire des Sciences du Climat et de l'Environnement, CNRS, Gif-sur-Yvette, France.

Corresponding author: F. M. Monteiro, School of Geographical Sciences, University of Bristol, University Road, Bristol BS8 1SS, UK. (f.monteiro@bristol.ac.uk)


0883-8305/12/2012PA002351

*and Köster*, 1998; *Tsikos et al.*, 2004; *Forster et al.*, 2008; *Sepúlveda et al.*, 2009; *Takashima et al.*, 2010]. Preceding OAE2 was an increase in volcanic and hydrothermal marine activity which potentially released large amounts of greenhouse gases into the atmosphere [*Adams et al.*, 2010; *Barclay et al.*, 2010; *Jenkyns*, 2010]. Large igneous provinces started to develop in particular at the Caribbean plateau and Madagascar traps less than 1 Myrs before the onset of OAE2 [*Courtillot and Renne*, 2003; *Snow et al.*, 2005; *Kuroda et al.*, 2007; *Turgeon and Creaser*, 2008; *Ando et al.*, 2009]. Reconstructions of atmospheric $CO_2$ suggest high concentrations before OAE2 and at its onset in the range of 500–3300 ppmv [*Bice et al.*, 2006; *Barclay et al.*, 2010; *Sinninghe Damsté et al.*, 2010; *Hay*, 2011]. In parallel, reconstructions of sea-surface temperature (SST) indicate strong warming with OAE2, where SST increased by about 5° possibly reaching 33–42° in the mid- and tropical latitudes [*Bice et al.*, 2006; *Forster et al.*, 2007; *Jenkyns*, 2010], and potentially more than 20° in the Arctic region [*Jenkyns et al.*, 2004]. Shortly after OAE2 onset, $pCO_2$ appears to have dropped by about 300 ppmv, a 10–50% decline [*Sinninghe Damsté et al.*, 2008; *Barclay et al.*, 2010; *Jarvis et al.*, 2011]. This decline is likely due to the increased carbon burial facilitated by the widespread of anoxia [*Jenkyns*, 2010].

[4] Since the discovery of the widespread deposition of black shales over 30 years ago [*Schlanger and Jenkyns*, 1976], the mechanisms responsible for OAE2 (and OAEs in general) remain a topic of intense debate [*Arthur and Sageman*, 1994; *Meyer and Kump*, 2008; *Jenkyns*, 2010]. Most consider either (1) a reduction in oxygen supply to the deep ocean allowing higher organic carbon preservation [*Schlanger et al.*, 1987; *Arthur and Sageman*, 1994], or (2) an increase in marine productivity which provided more organic matter to be respired, at the expense of oxygen (and other oxidants) in the water column, and to be buried in the sediments [*Schlanger and Jenkyns*, 1976; *Jenkyns*, 2010]. Both mechanisms (oxygen supply and marine productivity) could potentially explain the change of oceanic redox observed during OAE2. With increasing temperatures, the ocean would have experienced a decrease in oxygen solubility [*Arthur and Sageman*, 1994; *Kuypers et al.*, 2002] and, as speculated, a slowdown (or even stagnation) of the overturning ocean circulation [*Bralower and Thierstein*, 1984; *Arthur and Sageman*, 1994]. Warmer temperatures could also have increased marine productivity as a result of higher phytoplanktonic activity [*Eppley*, 1972]. Evidence exists for higher marine productivity in the tropics as shown from sediment barium content [*Kuypers et al.*, 2002] and assemblages of planktic foraminifera and calcareous nannofossils [*Premoli Silva et al.*, 1999; *Coccioni and Luciani*, 2005; *Hardas and Mutterlose*, 2007]. Recent observations of the North Atlantic Ocean and West Tethys Sea also suggest that marine productivity could have been stimulated by increased nutrient supply [*Kuypers et al.*, 2002; *Mort et al.*, 2007; *Jenkyns*, 2010].

[5] Understanding the mechanism of increased marine productivity, however, is not an easy task, because of the complexity of the marine ecosystem and its interaction with the nutrient cycles. Main limiting nutrients of the marine production include phosphate, fixed nitrogen (nitrate, ammonium, and nitrite) and iron. Evidence from total phosphorus accumulation rates in sediments suggest that the ocean phosphorus content increased right before the OAE2 onset [*Mort et al.*, 2007; *Kraal et al.*, 2010]. With warmer temperatures, continental weathering could have intensified and delivered more phosphate to the ocean via fluvial inputs [*Schlanger and Jenkyns*, 1976; *Jones and Jenkyns*, 2001; *Jenkyns*, 2010]. This higher weathering phosphorus supply is the key mechanism in recent box model studies to explaining the occurrence and periodicity of the OAEs during the Cretaceous [*Handoh and Lenton*, 2003; *Ozaki et al.*, 2011], an idea that still needs to be tested in a full 3D-ocean model representation. In addition, phosphate could have come from sediments once they became anoxic, via the preferential phosphorus regeneration relative to carbon [*Van Cappellen and Ingall*, 1994; *Bjerrum et al.*, 2006; *Tsandev and Slomp*, 2009; *Palastanga et al.*, 2011]. Therefore, enhanced marine productivity and carbon export could have been an important trigger of OAE2 via elevated phosphate concentrations of the ocean.

[6] Other nutrient cycles also experienced large changes during OAE2. In particular it has been suggested that the fixed nitrogen supply to the ocean increased during the event due to higher nitrogen fixation [*Kuypers et al.*, 2004a; *Meyers et al.*, 2009]. This is expected because strong rates of bacterial-mediated denitrification (the use of nitrate to remineralize organic matter) must have occurred with the spread of dysoxic/anoxic environments in the ocean [*Junium and Arthur*, 2007]. This would have removed fixed nitrogen from the oceans and favored nitrogen fixation [*Redfield*, 1958; *Monteiro et al.*, 2011; *Higgins et al.*, 2012]. As for iron, enhanced hydrothermal activity associated with OAEs could have provided more iron to the phytoplankton [*Arthur et al.*, 1987; *Kolonic*, 2005; *Snow et al.*, 2005]. Iron fertilization is however unlikely to be an important trigger of OAE2, because of a delay between the onsets of the large igneous provinces and OAE2 [*Turgeon and Creaser*, 2008; *Ando et al.*, 2009], or the potential of trace metal toxicity for marine organisms [*Erba*, 2004]. Finally, nutrient supply to the ocean surface might have also increased with changes in ocean circulation, potentially by increasing the strength of upwelling [*Poulsen et al.*, 2001; *Leckie et al.*, 2002; *Handoh et al.*, 2003; *Junium and Arthur*, 2007]. Overall, a range of changes in ocean biogeochemistry and physics could have potentially played a role in either causing or sustaining OAE2.

[7] Here we determine how changes in the oceanic supply in oxygen (including ocean circulation and oxygen solubility) and in marine productivity can bring about the observed oceanic redox changes associated with OAE2 using the Earth System model GENIE [*Ridgwell et al.*, 2007]. GENIE is a well designed model for this investigation because it can be run for hundreds of thousand years needed to equilibrate the ocean biogeochemistry, and accounts for the main 3-D features of ocean dynamics and biogeochemical cycles of the Late Cretaceous. We compile observations of redox changes of the global ocean, combining evidence of seafloor dysoxia/anoxia and photic zone euxinia (anoxic and free hydrogen sulfide) before and during OAE2. We then investigate in the model the impacts of paleogeography, oxygen supply and marine productivity on oceanic oxygen concentrations for different values of atmospheric $CO_2$ and oceanic phosphate inventory. The model results are compared with compiled

**Table 1.** Evidence of Seafloor Dysoxia/Anoxia Before and During OAE2[a]

| # | Locations | Low Oxygen | | Evidence | References |
|---|---|---|---|---|---|
| | | Pre | OAE2 | | |
| A | Cape Hatteras (DSDP sites 105, 603B) | ●? | ● | Pre: Succession of bioturbated green claystone and laminated black shales, TOC < 10% OAE2: Laminated black shales, 3.5–26% TOC, absence ofbenthic foraminifera | *Sinninghe Damsté and Köster* [1998]; *Kuypers et al.* [2004b]; *Pancost et al.* [2004] |
| B | Newfoundland Basin (ODP Site 1276) | | ● | OAE2: Laminated black shales, up to 13.4% TOC | *Sinninghe Damsté et al.* [2010] |
| C | Hatteras Abyss (DSDP site 417) | | ● | OAE2: Laminated black shales, 6% TOC | *Sinninghe Damsté and Köster* [1998] |
| D | Tarfaya Basin (Morocco) | ● | ● | Pre: Laminated black shales, 2–5% TOC OAE2: Laminated black shales, 1–20% TOC | *Schlanger et al.* [1987]; *Sinninghe Damsté and Köster* [1998]; *Holbourn and Kuhnt* [2002]; *Kolonic et al.* [2002]; *Kuypers et al.* [2002]; *Lüning et al.* [2004]; *Tsikos et al.* [2004]; *Kolonic* [2005]; *Mort et al.* [2008] |
| E | Maracaibo Basin (Venezuela) | ● | ● | Pre: Succession of laminated marlstone and chert, 10–14% TOC OAE2: Laminated marlstone, 7–11% TOC | *Schlanger et al.* [1987]; *Perez-Infante et al.* [1996] |
| F | Demerara Rise (DSDP site 144, ODP Leg 207) | ● | ● | Pre: Claystones and laminated black shales, 1–13% TOC OAE2: Laminated black shales, 5–32.5% TOC, euxinic sediments | *Sinninghe Damsté and Köster* [1998]; *Kuypers et al.* [2002]; *Kuroda and Ohkouchi* [2006]; *Junium and Arthur* [2007]; *Arndt et al.* [2009]; *Hetzel et al.* [2009]; *Meyers et al.* [2009] |
| G | Cape Verde (DSDP sites 367, 368) | ● | ● | Pre: 9% TOC OAE2: Laminated black shales, 6.5–50% TOC | *Sinninghe Damsté and Köster* [1998]; *Kuypers et al.* [2002]; *Lüning et al.* [2004]; *Sinninghe Damsté et al.* [2008] |
| H | Angola Basin (DSDP site 530A) | × | ● | Pre: Bioturbated red and green claystone, low TOC OAE2: Laminated black shales, >25% TOC, low bioturbation | *Forster et al.* [2008] |
| J | Eastbourne and Dover (UK) | × | × | Pre and OAE2: Bioturbated chalk, <0.25% TOC, benthic foraminifera | *Jarvis et al.* [1988]; *Gale et al.* [2000]; *Tsikos et al.* [2004] |
| K | Münsterland Basin (Germany) | × | × | Pre: Limestone, <1% TOC OAE2: Succession of limestone, marlstone and homogeneous black shales, <3% TOC, rich assemblage in benthic foraminifera | *Schlanger et al.* [1987]; *Hilbrecht et al.* [1992]; *Holbourn and Kuhnt* [2002]; *Voigt et al.* [2007] |
| L | Chrummflueschluch (Switzerland) | × | × | Pre and OAE2: Limestone, low TOC | *Westermann et al.* [2010] |
| M | Vocontian Basin (France) | × | ● | Pre: Marlstone, <1% TOC, rich assemblage in benthic foraminifera OAE2: Succession of homogeneous and laminated black shales, 5% TOC, low benthic foraminifera content | *Schlanger et al.* [1987]; *Holbourn and Kuhnt* [2002]; *Takashima et al.* [2009] |
| N | Galicia Margin (ODP Site 641) | | ● | OAE2: Laminated black shales, 6.5–11% TOC | *Sinninghe Damsté and Köster* [1998]; *Lüning et al.* [2004]; *Pancost et al.* [2004] |
| P | Apennines (Italy) | × | ● | Pre: Light pelagic limestone OAE2: Laminated black shales, 12–26% TOC | *Schlanger et al.* [1987]; *Salvini and Passerini* [1998]; *Sinninghe Damsté and Köster* [1998]; *Luciani and Cobianchi* [1999]; *Pancost et al.* [2004]; *Tsikos et al.* [2004]; *Mort et al.* [2007] |
| Q | Oued Bahloul (Tunisia) | × | ● | Pre: Bioturbated limestone, rich assemblage in benthic foraminifera OAE2: Laminated black shales, 1–6% TOC, low benthic foraminifera content | *Schlanger et al.* [1987]; *Lüning et al.* [2004]; *Pancost et al.* [2004]; *Ohkouchi et al.* [2006]; *Nederbragt and Fiorentino* [1999] |
| R | Levant Platform (Jordan) | × | ● | Pre: Marlstone, <1% TOC OAE2: Marlstone, 1.5–3% TOC | *Sepúlveda et al.* [2009] |
| S | Tethyan Himalayas (Tibet) | × | ●? | Pre: Dark shales and marlstone, benthic foraminifera OAE2: Laminated black shales, <2% TOC, low benthic foraminifera content, and gray bioturbated limestone (in shallow waters) | *Wang et al.* [2001]; *Wan et al.* [2003]; *Li et al.* [2009] |
| T | Kerguelen Plateau (ODP site 1138) | | ■ | OAE2: Laminated black shales, up to 3% TOC, low benthic foraminifera content, abundant authigenic pyrite | *Holbourn and Kuhnt* [2002] |

**Table 1.** (continued)

| # | Locations | Low Oxygen | | Evidence | References |
|---|---|---|---|---|---|
| | | Pre | OAE2 | | |
| U | Yezo Group (Japan) | × | ●? | Pre: Bioturbated mudstones OAE2: Weakly bioturbated mudstones, <1% TOC, lack of macrofossils, extinction of benthic foraminifera, dense occurrence of pyrite and radiolarians | *Kaiho and Hasegawa* [1994]; *Takashima et al.* [2010] |
| V | Mariana Basin (DSDP site 585) | + | ■? | Pre: Chalk, claystone and siltstone OAE2: Pyritic black shales, 10% TOC, turbidite section | *Schlanger et al.* [1987] |
| W | Shatsky and Hess Rises (DSDP sites 305, 310) | | ■? | OAE2: Bituminous and laminated-pyritic black shales, 9.3% TOC, absence of benthic foraminifera, poor core recovery | *Schlanger and Jenkyns* [1976]; *Schlanger et al.* [1987] |
| X | Central South Pacific (DSDP site 463) | × | × | Pre and OAE2: Succession of chalk and common chert, <1% TOC | *Ando et al.* [2009] |

[a]The evidence for is represented by black dots and squares (●, ■); evidence against by crosses (×, +). Interrogation marks (?) indicate the evidence possibility. Evidence for (or against) combines observations of laminated (or bioturbated) sediments, high (or low) organic-carbon content and low (or high) concentration of benthic foraminifera. We associate pre-OAE2 conditions with observations immediately preceding the positive carbon isotope excursion, and OAE2 conditions with the observed peak in dysoxia/anoxia from the plateau of maximum excursion. For locations which do not have carbon isotope measurements, we associate the OAE2 interval with the planktic foraminifera *W. archaeocretacea* biozone and indicates this biostratigraphic definition with black squares (■) and vertical crosses (+).

observations to estimate the minimum extent of anoxia during OAE2 and to assess which mechanisms may have contributed to the observed changes in oceanic redox state across OAE2.

## 2. Observations of Marine Biogeochemical Changes Across OAE2

[8] *Schlanger and Jenkyns* [1976] were the first to infer that OAE2 experienced large changes in oxygen and carbon cycles. Their reconstruction combined lithostratigraphic and biological data suggesting a brief but geographically widespread expansion of seafloor anoxia across OAE2. Subsequently, geochemical proxies have been applied to OAE2 sediments and revealed redox changes in the photic zone [e.g., *Sinninghe Damsté and Köster*, 1998] or sediments [e.g., *Kraal et al.*, 2010]. We combine these observations with more recent evidence and provide an up-to-date overview of the Cenomanian-Turonian changes in seafloor dysoxia/anoxia (Table 1 and Figures 1b and 1c) and photic zone euxinia (Table 2 and Figures 1d and 1e).

[9] We define pre-OAE2 and OAE2 conditions on the basis of observations from sediments immediately preceding the positive carbon isotope excursion (CIE) and from sediments deposited during the plateau of the maximum CIE, respectively. For locations which do not have carbon isotope measurements, we define OAE2 conditions using observations from sediments deposited within the planktic foraminiferal *Whiteinella archaeocretacea* biozone, a biostratigraphic zone often recognized to capture most of the CIE [*Jarvis et al.*, 1988; *Hilbrecht et al.*, 1992; *Kuypers et al.*, 2002; *Kolonic*, 2005]. We acknowledge this difference of OAE2 definition in our compilation. For simplification, we do not attempt to capture the temporal variations that occur during the CIE either within or between locations, as has been observed for example in TOC contents in the Tethys Sea and equatorial proto-Atlantic Ocean [*Tsikos et al.*, 2004; *Kraal et al.*, 2010]. Instead we define OAE2 conditions at a given site on the basis of the peak redox change and only report the strongest evidence for seafloor dysoxia/anoxia and photic zone euxinia at that site. For example, we define the Tarfaya Basin as being characterized by seafloor anoxia during OAE2, even though black shale deposition is episodic [*Kolonic*, 2005]. Finally, we do not include observations from the Arctic Ocean and Western Interior Seaway, because our model resolution is too low in these regions to be able to reconstruct the observed patterns. Overall, the North and equatorial proto-Atlantic Ocean and the West Tethys Sea present the best data coverage across the event. Little coverage exists in the proto-South Atlantic Ocean, East Tethys Sea and Indian Ocean, with very limited coverage in the Pacific Ocean, potentially restricting our reconstruction of the oceanic redox OAE2 changes in these regions.

### 2.1. Evidence for Seafloor Redox Conditions

[10] Seafloor oxygenation can qualitatively be evaluated from observations of total organic carbon (TOC) combined with descriptions of sedimentary structure (laminated or bioturbated) and benthic foraminiferal abundance [*Schlanger and Jenkyns*, 1976; *Arthur and Sageman*, 1994]. In well-oxygenated environments, sediments rarely preserve more than 0.5% TOC [*Demaison and Moore*, 1981; *Arthur and Sageman*, 1994], and TOC contents above 1% are usually interpreted as a signature of dysoxic/anoxic conditions at the seafloor, albeit not necessarily anoxic when observed in ocean basin settings [*Schlanger et al.*, 1987; *Lüning et al.*, 2004]. Laminated sediments indicate that the deposition occurred with a restricted benthic community, limiting bioturbation. Laminated sediments as well as low benthic foraminiferal abundance have then been argued to be evidence for limited oxygen supply to the sediments, although a smaller biological community can also result from a lack of organic matter inputs [*Schlanger et al.*, 1987]. Finally, the presence of authigenic pyrite can be interpreted as evidence for sulfate reduction hence anoxia in shallow sediments [*Wignall and Newton*, 1998]. We compile these different indicators of seafloor dysoxia/anoxia for pre-OAE2 and OAE2 intervals (Table 1 and Figures 1b and 1c).

[11] The evidence is marked as 'questionable' in cases where the indicators of dysoxia/anoxia are equivocal, for

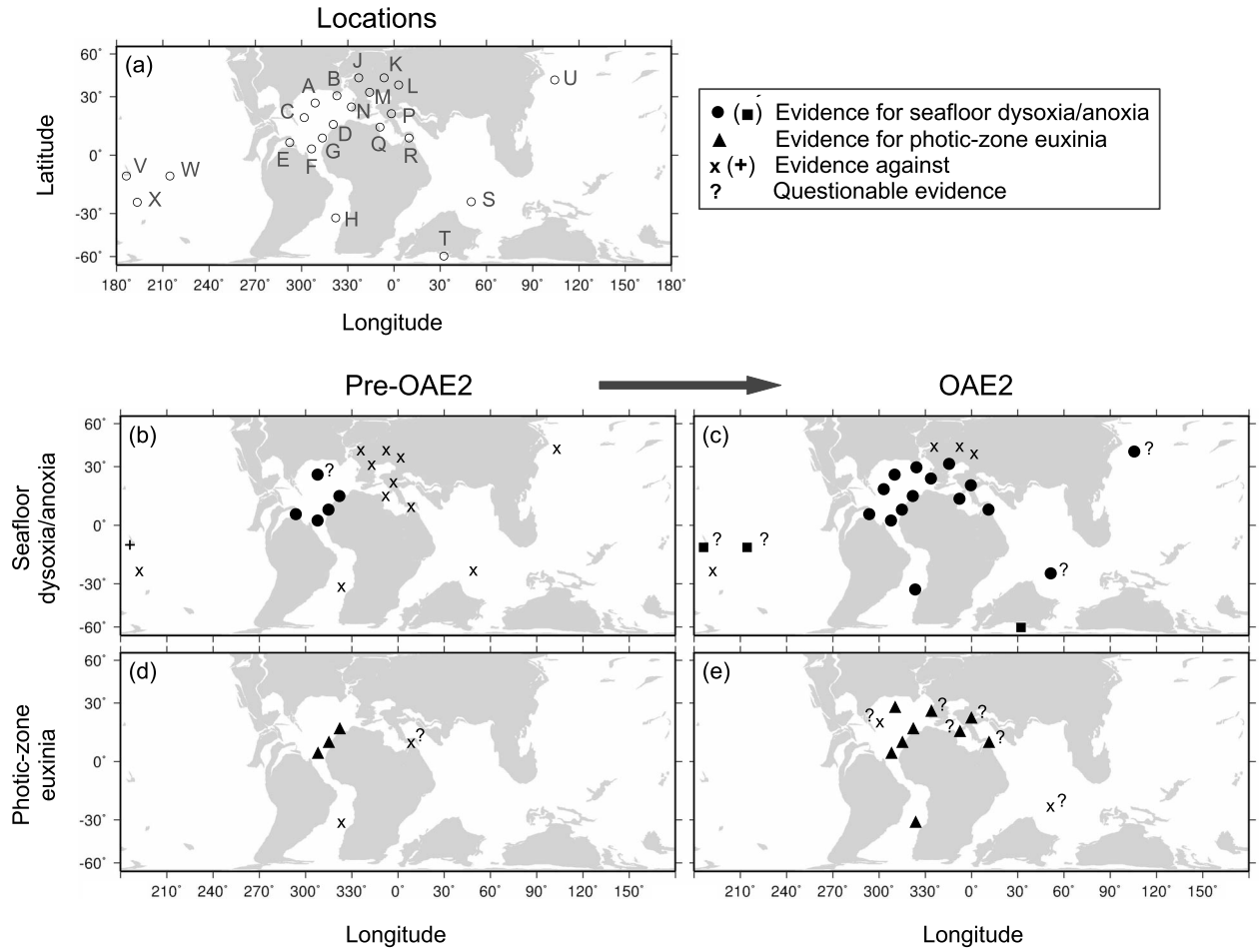


**Figure 1.** Observations in oceanic redox changes before and during OAE2. We associate pre-OAE2 conditions with observations immediately preceding the positive carbon isotope excursion, and OAE2 conditions with the observed redox peak from the plateau of maximum excursion. (a) Locations of the observations as described in Tables 1 and 2 (map available at http://www.odsn.de/odsn/services/paleomap/paleomap.html); (b, c) Evidence of seafloor dysoxia/anoxia. Black dots and squares indicate evidence for, crosses and plus signs indicate evidence against, and question marks indicate the uncertainty in the evidence. For locations with no carbon isotope measurements, the OAE2 interval is associated with the *W. archaeocretacea* biozone and distinguished by black squares and plus signs; (d, e) Evidence for photic zone euxinia. Black triangles indicate evidence for, crosses indicate evidence against, and question marks indicate the uncertainty in the evidence.

example, for sediments characterized by low bioturbation and benthic foraminifera abundance but also low TOC contents such as in the Tethyan Himalayas and Yezo Group (locations S, U). We also consider as questionable, observations from the equatorial Pacific Ocean because of the presence of turbidite in the OAE2 section at DSDP site 585 (location V) and of poor core recovery inducing poorly constrained dating at DSDP sites 305/310 (location W), as discussed by *Sliter* [1995].

[12] Collectively, observations show that prior to OAE2 the seafloor of the proto-North Atlantic Ocean was already dysoxic/anoxic (Figure 1b). This is reflected by the presence of relatively high TOC contents and laminated black shales at DSDP sites 105/603B, 144 and 367/368 (locations A, F, G, check Table 1 for references and hereafter), and at the Tarfaya Basin and the Maracaibo Basin (locations D, E). In contrast, the seafloor of the Tethys Sea, and the proto-South Atlantic, Indian and Pacific Oceans appear to have been oxic prior to the event. This is suggested by low TOC contents, bioturbated sediments and high benthic foraminifera abundances at for instance DSDP site 530A, Eastbourne/Dover, the Apennines, Oued Bahloul and Yezo Group (locations H, J, P, Q, U). During OAE2, seafloor dysoxia/anoxia spread across much of the globe for which rock records have been studied. The proto-South Atlantic Ocean, most of the Tethys Sea, and parts of the Indian Ocean and the Northwest and equatorial Pacific Ocean were most likely dysoxic/anoxic during the event, suggested by the presence of laminated black shales and low benthic foraminiferal abundances. Places where oxic conditions persisted during OAE2 are mainly in shallow waters characteristic of the northern Tethys area such as Eastbourne/Dover, the Münsterland Basin and Chrummueschluch in the Swiss Alps (locations J, K, L). These areas are characterized by low-TOC chalk or

**Table 2.** Evidence of Photic Zone Euxinia of the Ocean Before and During OAE2[a]

| # | Locations | Euxinia | | Evidence | References |
|---|---|---|---|---|---|
| | | Pre | OAE2 | | |
| A | Cape Hatteras (DSDP sites 105, 603B) | | ▲ | OAE2: Isorenieratane, Me,*i*-Bu maleimide | *Kuypers et al.* [2004b]; *Pancost et al.* [2004]; not in *Sinninghe Damsté and Köster* [1998] |
| C | Hatteras abyss (DSDP site 417) | | ×? | OAE2: Absence of isorenieratane (low resolution) | *Sinninghe Damsté and Köster* [1998] |
| D | Tarfaya Basin (Morocco) | ▲ | ▲ | Pre: Isorenieratane OAE2: Isorenieratane | *Sinninghe Damsté and Köster* [1998]; *Kolonic et al.* [2002]; *Kuypers et al.* [2002]; *Kolonic* [2005] |
| F | Demerara Rise (DSDP site 144, ODP Leg 207) | ▲ | ▲ | Pre: Isorenieratane OAE2: Isorenieratane | *Sinninghe Damsté and Köster* [1998]; *Kuypers et al.* [2002] |
| G | Cape Verde (DSDP sites 367, 368) | ▲ | ▲ | Pre: Isorenieratane OAE2: Isorenieratane, Me,*i*-Bu maleimide | *Sinninghe Damsté and Köster* [1998]; *Kuypers et al.* [2002]; *Pancost et al.* [2004] |
| H | Angola Basin (DSDP site 530A) | × | ▲ | Pre: Absence of S-bound isorenieratane OAE2: Isorenieratane (with lower values than in North proto-Atlantic) | *Forster et al.* [2008] |
| N | Galicia Margin (ODP site 641) | | ▲? | OAE2: Absence of isorenieratane (low resolution), low Me,*i*-Bu maleimide content, absence of thermal maturity | *Sinninghe Damsté and Köster* [1998]; *Pancost et al.* [2004] |
| P | Apennines (Italy) | | ▲? | OAE2: Absence of isorenieratane, Me,*i*-Bu maleimide, high thermal maturity | *Sinninghe Damsté and Köster* [1998]; *Pancost et al.* [2004] |
| Q | Oued Bahloul (Tunisia) | | ▲? | OAE2: Me,*i*-Bu maleimide (in 50% of localities) | *Pancost et al.* [2004] |
| R | Levant Platform (Jordan) | ×? | ▲? | Pre: Absence of isorenieratane (low resolution), low gammacerane level OAE2: Absence of isorenieratane (low resolution), high gammacerane level | *Sepúlveda et al.* [2009] |
| S | Tethyan Himalayas (Tibet) | | ×? | OAE2: Large size of pyrite framboids | *Wan et al.* [2003] |

[a]Evidence for combine observations of green sulfur bacteria biomarkers (isorenieratane, Me,*i*-Bu maleimide), ciliate biomarker (gammacerane) and pyrite framboid size distribution. Evidence for dysoxia is represented by black triangles (▲); evidence against by crosses (×). Interrogation marks (?) indicate the evidence possibility.

limestone, as well as high benthic foraminifera abundance. The South central Pacific Ocean might have also had a persistently oxic seafloor as indicated by deposition of low-TOC chalk and chert in the Central South Pacific Ocean at DSDP site 463 (location Y). However, this site is located in the middle of an open ocean subtropical gyre, so that the lack of organic carbon burial could be due to low productivity and organic matter inputs.

[13] Our new compilation of observations is consistent with previous interpretations (reviewed in *Jenkyns* [2010]) that during OAE2 the deep ocean experienced large variations in oxygenation. Yet, the lack of data for most parts of the Cretaceous oceans means that uncertainties still remain on how global the perturbation was. This is particularly relevant for the Pacific Ocean which has the poorest data reconstruction, though the largest ocean basin of the Late Cretaceous.

### 2.2. Evidence for Photic Zone Euxinia

[14] Evidence for photic zone euxinia provides another constraint of the reconstruction of OAE2 oceanic redox changes. Euxinia describes any environment containing free hydrogen sulfide ($H_2S$), which is characteristic of anoxia. $H_2S$ is produced by sulfate reduction under anoxic conditions and is readily oxidized when exposed to oxygen. Evidence for euxinia mainly come from biomarkers for green sulfur bacteria (GSB), which indicate euxinia in the photic zone as these bacteria require both light and $H_2S$ [e.g., *Summons and Powell*, 1987; *Sinninghe Damsté and Köster*, 1998]. Two main types of GSB biomarkers have been measured in Mesozoic sediments: isorenieratane, a derivative of the carotenoid isorenieratene [*Sinninghe Damsté and Köster*, 1998; *Kuypers et al.*, 2002; *Pancost et al.*, 2004], and Me,*i*-Bu maleimides, a bacteriochlorophyll-based structure [*Pancost et al.*, 2004; *Sepúlveda et al.*, 2009]. Isorenieratane can particularly occur as free hydrocarbon or S-bound/S-bearing analogs, arising from reactions of isorenieratene double bonds with reduced inorganic S species [*Kuypers et al.*, 2002]. Gammacerane is also used as evidence for photic zone euxinia as a triterpenoid biomarker derived from ciliates that potentially grazed on GSB [*Sinninghe Damsté et al.*, 1995]. Finally evidence for euxinia in the water column, although not necessarily in the photic zone, can come from pyrite framboids for which a small size range (<6 $\mu$m in diameter) is generally interpreted as arising from rapid precipitation in euxinic waters [*Wignall and Newton*, 1998; *Wan et al.*, 2003]. We compile and present the evidence of the photic zone euxinic states for before and during OAE2 based on the presence of biomarkers and pyrite (Table 2 and Figures 1d and 1e).

[15] The evidence is marked as 'questionable' when the observation relies only on Me,*i*-Bu maleimides (particularly when concentrations are low), gammacerane or pyrite framboids, because alternative explanations for these

observations are possible. For example, ancient sediments are typically characterized by a range of maleimides with extended alkyl moieties (>C4), including branched components with no known biological source [e.g., *Pancost et al.*, 2004]; although their origin is unclear, it could be diagenetic, which by extension suggests a potential analogous diagenetic origin of Me,*i*-Bu maleimide. Alternative origins for isorenieratane have not been proposed, and even in isolation, its occurrence is presented as evidence for photic zone euxinia. However, we do note that other processes, such as lateral transport of sediment, could account for the presence of isorenieratane in some sediments.

[16] The available observations for photic zone euxinia is more limited than for seafloor anoxia (especially prior to OAE2 as shown in Figure 1). However, clear spatial relationships occur as previously noted [*Jenkyns*, 2010]. Prior to OAE2 (Figure 1d), the photic zone of the equatorial proto-Atlantic Ocean was already euxinic, reflected by the presence of GSB biomarkers at Tarfaya Basin and DSDP sites 144 and 367/368 (locations D, F, G). This contrasts with the proto-South Atlantic Ocean and Southwest Tethys Sea at DSDP site 530A and the Levant Platform (locations H, R), where isorenieratane was not detected (though Me,*i*-Bu maleimides have not been examined at those sites). During OAE2, euxinic photic zone waters also occupied the tropical proto-South Atlantic Ocean and the northernmost proto-Atlantic, as indicated by the presence of isorenieratane at DSDP sites 105/603B and 530A (locations A, H). Euxinia might have also reached the photic zone of the Southwest Tethys Sea, as indicated by the presence of GSB biomarkers at DSDP site 641, the Apennines, Oued Bahloul and Levant Platform (locations A, N, P, Q, R). These last observations are, however, uncertain because the evidence in most of these locations relies only on gammacerane and/or Me,*i*-Bu maleimide.

[17] Together, sedimentary, biomarker and geochemical data across OAE2 indicate that seafloor dysoxia/anoxia expanded from the proto-North Atlantic Ocean to most ocean basins of the Late Cretaceous, and photic zone euxinia from the equatorial proto-Atlantic Ocean to most of the proto-Atlantic Ocean and Southwest Tethys Sea. photic zone euxinia probably indicates a lack of oxygen and nitrate in the lower photic zone and potentially in underlying waters [e.g., *Sinninghe Damsté and Köster*, 1998], because organic matter remineralization by sulfate reduction only occurs once oxygen and nitrate are both depleted. However, the interpretation of euxinic conditions in deeper waters is somewhat contentious, because euxinic conditions could have been restricted to a surface water oxygen minimum zone while intermediate waters remained oxic.

## 3. Model Description

[18] Oceanic redox states for before and during OAE2 are reconstructed using the Earth System model GENIE [*Ridgwell et al.*, 2007]. GENIE is a frictional-geostrophic 3D-ocean model coupled to an energy-moisture balance 2D-atmosphere model [*Edwards and Marsh*, 2005]. The ocean model has a 36x36 equal-area horizontal grid and 16 vertical levels similar to GENIE-16 presented by *Cao et al.* [2009]. We configure GENIE for the Late Cretaceous using Cenomanian bathymetry and continental configuration, both derived from the higher resolution model FOAM simulations of *Donnadieu et al.* [2006] which used *Sewall et al.*'s [2007] boundary conditions (Figure 2). The annual average wind stress field transformed to the GENIE grid comes from the Cenomanian FOAM experiment run with 4 × CO2 (relative to the preindustrial atmospheric value). A simple zonal planetary albedo distribution is applied, derived from the Late Cretaceous GCM experiment of *Hunter et al.* [2008]. The solar constant is reduced by 0.56% appropriate for the Late Cretaceous. Despite its lower resolution, GENIE captures the commonly described features of the Late Cretaceous ocean circulation, including major gyres and equatorial westward currents at the surface, and deep-water formation in the North Pacific and Southern Oceans [*Poulsen et al.*, 2001; *Trabucho Alexandre et al.*, 2010; *Murphy and Thomas*, 2012]. The lower resolution is key to running a 3D-ocean model for 10 kyrs or more, which is necessary to examine regional differences in, and the effect of ocean circulation on, the Cretaceous biogeochemistry.

[19] GENIE includes the biogeochemical cycling of carbon, phosphorus, nitrogen, oxygen and sulfur as described by *Ridgwell et al.* [2007]. In addition here, we implement a temperature control on marine productivity and a more complete cycling of nitrogen, by including processes of nitrification (oxidation of ammonium into nitrate) as in *Fennel et al.* [2005], and nitrogen fixation (assimilation of $N_2$ by diazotrophs). See the auxiliary material for full description of the marine productivity and nitrogen cycle.[1] Sediments are not represented in this particular GENIE setup. Organic matter burial and phosphorus regeneration under anoxic condition are therefore not accounted for, but are very simply parameterized by fixing the global ocean phosphate inventory. The phosphate inventory is maintained through the model simulations by assuming all organic phosphorus reaching the seafloor to be instantaneously returned to phosphate at the bottom of the model ocean.

[20] We run different sets of numerical experiments to explore the impact of paleogeography, oxygen supply and marine productivity on the oceanic redox state across OAE2. The REFERENCE experiment has a Late Cretaceous configuration but is set with modern oceanic phosphate concentration ($1 \times$ PO4 = 2.15 $\mu$mol P $l^{-1}$) and pre-industrial atmospheric $CO_2$ ($1 \times$ CO2 = 278 ppmv). In the SENSITIVITY experiments, atmospheric $CO_2$ concentration varies from 1 to 16 times pre-industrial value ($1 \times -16 \times$ CO2) and oceanic $PO_4^{3-}$ concentration from 0.5 to 5 times modern value ($0.5 \times -5 \times$ PO4). The atmospheric $CO_2$ experiments aim to reveal the impact of oxygen supply and marine productivity with warming temperature, whereas the oceanic $PO_4^{3-}$ experiments aim to reveal the impact of marine productivity with increasing nutrient inventory. Finally to assess the impact of temperature on marine productivity, we run the NOBIOTEMP experiments, similar to the SENSITIVITY experiments where the phytoplankton growth is set independent of temperature. The REFERENCE experiment is initialized with modern ocean distribution and used to initialize other simulations. All simulations are run for 20 kyrs to steady state. Most simulations reach steady state after 10 kyrs

[1] Auxiliary materials are available in the HTML. doi:10.1029/2012PA002351.

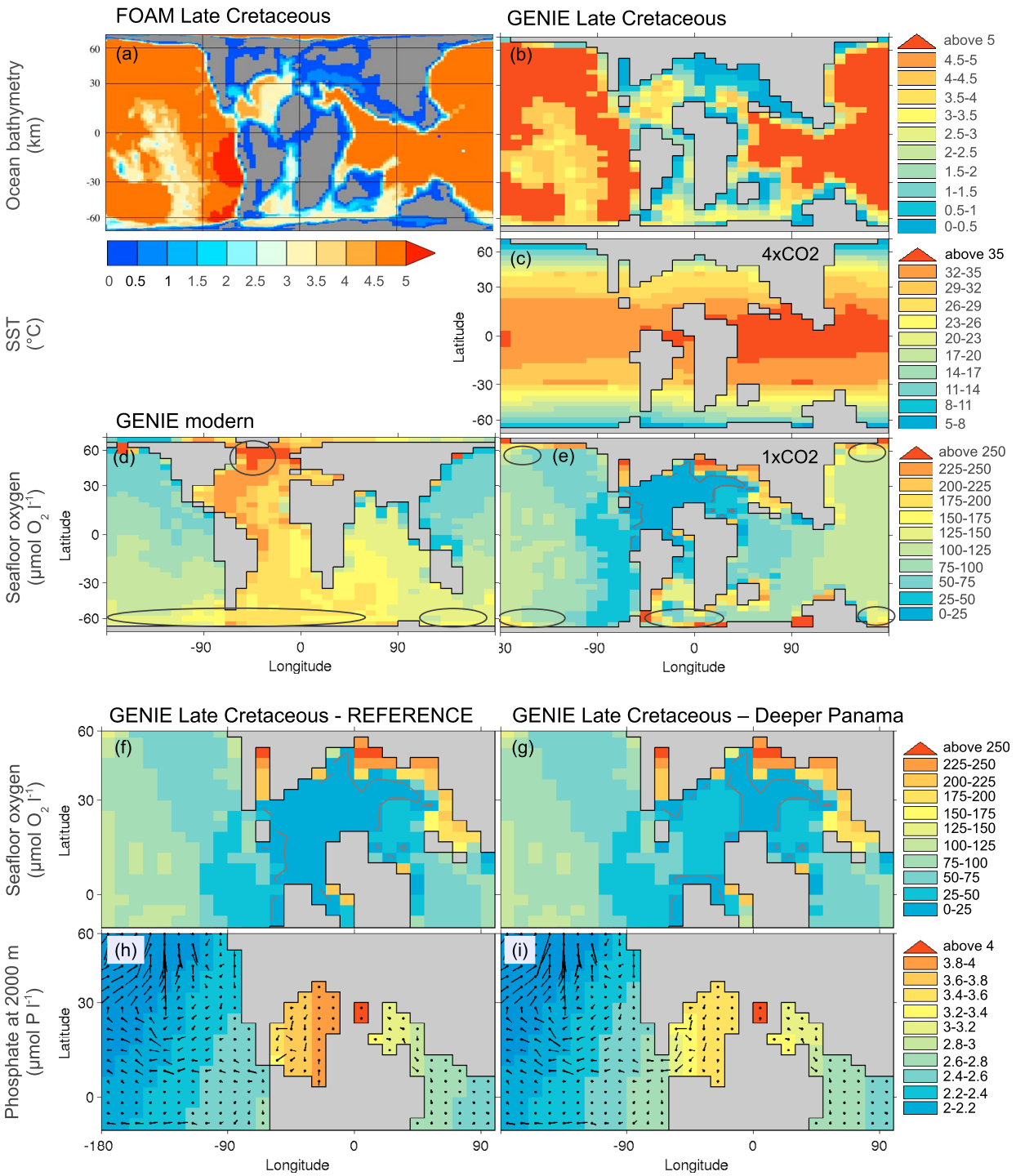


**Figure 2.** Model configuration for the Late Cretaceous and comparison of seafloor oxygen distribution with modern configuration and with deeper Panama gateway. Black circles indicate the areas of deep-water formation (from convective adjustment; Figures 2d and 2e). Gray contour indicates the model oxygen concentration of 10 $\mu$mol $O_2$ $l^{-1}$, delimiting the region of seafloor dysoxia/anoxia (panels Figures 2e–2g). (a) Cenomanian ocean bathymetry in the higher resolution model FOAM [*Donnadieu et al.*, 2006]; (b) GENIE ocean bathymetry for the Cenomanian rescaled from FOAM; (c) GENIE annual mean sea-surface temperature (SST) for 4 × CO2; (d) GENIE seafloor oxygen concentration with modern configuration; (e) GENIE seafloor oxygen concentration with Late Cretaceous configuration as in REFERENCE experiment; (f) REFERENCE seafloor oxygen concentration zoomed into the proto-North Atlantic basin; (g) Seafloor oxygen concentration for REFERENCE experiment with Panama gateway deepened to 3000 m (from 1500 m); (h) REFERENCE phosphate concentration (in color) and ocean currents (plotted on top, direction starts from the dot) at 2000 m; (i) Deeper Panama REFERENCE phosphate concentration and ocean currents at 2000 m.

except for simulations set with high atmospheric $CO_2$ concentrations.

## 4. Model Results

[21] We reconstruct the redox states of the Late Cretaceous ocean for before and during OAE2 by constraining the model results with the compiled observations. Modeled dysoxic/anoxic conditions are defined by oxygen concentrations lower than 10 $\mu$mol $O_2$ $l^{-1}$ [*Arthur and Sageman*, 1994], and photic zone euxinia by the occurrence of free hydrogen sulfide ($H_2S > 0$) in the sub-surface (80–200 m). We investigate first the impact of climatic changes in the model on the oceanic oxygen distribution of the Late Cretaceous.

### 4.1. Sensitivity of Oxygen in the Late Cretaceous Ocean

[22] The distribution of oxygen in the ocean relies on its supply from air-sea gas exchange between the atmosphere and the ocean combined with ocean circulation, and its removal via remineralization of organic matter. Paleogeography influences both ocean circulation and remineralization, whereas temperature impacts the solubility of oxygen (thus the air-sea gas exchange), ocean circulation and marine productivity, and nutrients impact marine productivity. As a result, the distribution of oxygen in the ocean is likely to vary with changes in paleogeography, temperature, and/or nutrient inventory. We examine these three parameters in the following sections.

#### 4.1.1. Role of Paleogeography

[23] The Late Cretaceous paleogeography differs significantly from a modern configuration, notably with respect to a smaller North Atlantic basin, an equatorial circumglobal current (via the Tethys Sea and an opened Panama gateway) and a restricted Southern Ocean. As a result, the distribution of dissolved oxygen in the Late Cretaceous ocean are markedly different from those of the modern ocean, particularly for the deep ocean. This can be evaluated by considering our Late Cretaceous REFERENCE experiment where atmospheric $CO_2$ and oceanic $PO_4^{3-}$ are set to modern values ($1 \times$ CO2 and $1 \times$ PO4) hence keeping temperature and marine productivity comparable. In this scenario, seafloor oxygen concentrations are also lower in the North Atlantic Ocean and higher in the Pacific Ocean of the Late Cretaceous (Figure 2e), a pattern almost opposite to the one of the modern ocean (Figure 2d). This difference in oxygen pattern arises from the influence of continental geography on the trajectory of water masses.

[24] The Late Cretaceous has a North Atlantic basin more inclined to be anoxic than today for two main reasons. First, in the Late Cretaceous, deep-water masses form in the polar regions of the Pacific Ocean [*Poulsen et al.*, 2001; *Hague et al.*, 2012] instead of in the North Atlantic Ocean as they do today (Figures 2d and 2e). This is a consequence of the northern extent of the Atlantic Ocean being further south (about 50°N) than in the modern ocean (about 65°N), which limits the effect of cooling on surface water density in the winter. The water masses traveling into the North Atlantic Ocean of the Late Cretaceous are therefore older, have experienced more remineralization, and hence are poorer in oxygen than for the modern case. Secondly, the proto-North Atlantic Ocean of the Late Cretaceous was a silled basin (Figure 2b), and this enclosed shape limits the ventilation of water masses in the deep ocean. The content of oxygen in the proto-North Atlantic Ocean is for instance sensitive to the deepening of the Panama gateway. When deeper, the proto-North Atlantic Ocean, though still less oxic than in the modern case, stops being anoxic (Figures 2f and 2g). This is because deep currents from the Pacific Ocean invade the Atlantic Ocean, bringing oxygen-rich and nutrient-poor waters to the proto-North Atlantic Ocean (Figures 2h and 2i). This model result is against the estuarine circulation mechanism suggested to be at the origin of black shale deposition in this region where anoxia is sustained by an inflow of nutrient-rich water [*Meyer and Kump*, 2008; *Trabucho Alexandre et al.*, 2010]. Our model experiment is more aligned with *Demaison and Moore*'s [1981] open-ocean mechanism by which proto-North Atlantic anoxia relates to the distance from deep-oxygenated water sources. Our model suggests that the Late Cretaceous paleogeography is responsible for the favored deposition of black shales in the proto-North Atlantic Ocean, the only region observed to have seafloor dysoxia/anoxia prior to OAE2.

#### 4.1.2. Role of Increasing Temperature and Ocean Nutrient Content

[25] We illustrate the impact of temperature on oxygen supply (or ocean physics) for the Late Cretaceous using the NOBIOTEMP experiments where the temperature effect on marine productivity is switched off. In these experiments, when oceanic phosphate concentration is held constant ($1 \times$ PO4), increasing $pCO_2$ from $1 \times$ CO2 to $16 \times$ CO2 causes the globally averaged sea-surface temperature to warm from 23° to 34° (Figure 3b). This increase causes the globally averaged oceanic oxygen concentration to drop by about 25% (from 110 to 80 $\mu$mol $O_2$ $l^{-1}$) and dysoxia/anoxia to expand from 8% to about 11% of the global seafloor area. This oxygen decline is mainly due to the decrease in oxygen solubility. Our modeled ocean circulation does not vary significantly with increasing $pCO_2$ (Figure 3a), which is consistent with results from a higher resolution ocean model of the Cretaceous [*Poulsen et al.*, 2001]. A previous study, based on a similar intermediate-complexity ocean model of the Late Cretaceous, suggests that, in contrast, ocean circulation slowed with increasing $pCO_2$ and, in fact, can shut down totally at $16 \times$ CO2 levels for a duration of 1,300 yrs [*Misumi and Yamanaka*, 2008]. We also observed that the overturning circulation in GENIE becomes shallower for the first 500 yrs following the warming. While the slowing of ocean circulation associated with warming might have helped trigger some anoxia for OAE2, we expect that it has a minor influence because of its transient state in comparison to the OAE2 interval (250–700 kyrs).

[26] The effect of temperature on marine productivity is illustrated by contrasting SENSITIVITY with NOBIOTEMP experiments while keeping oceanic phosphate constant ($1 \times$ PO4). Including this productivity effect causes the geographical area of seafloor dysoxia/anoxia to increase by about another 0.5–1% (shown by the difference between Figures 3b and 3c). This intensification is rather small in comparison to the impact of ocean physics alone. Therefore, for marine productivity to be a potential driver of OAEs, other parameters have to be invoked.

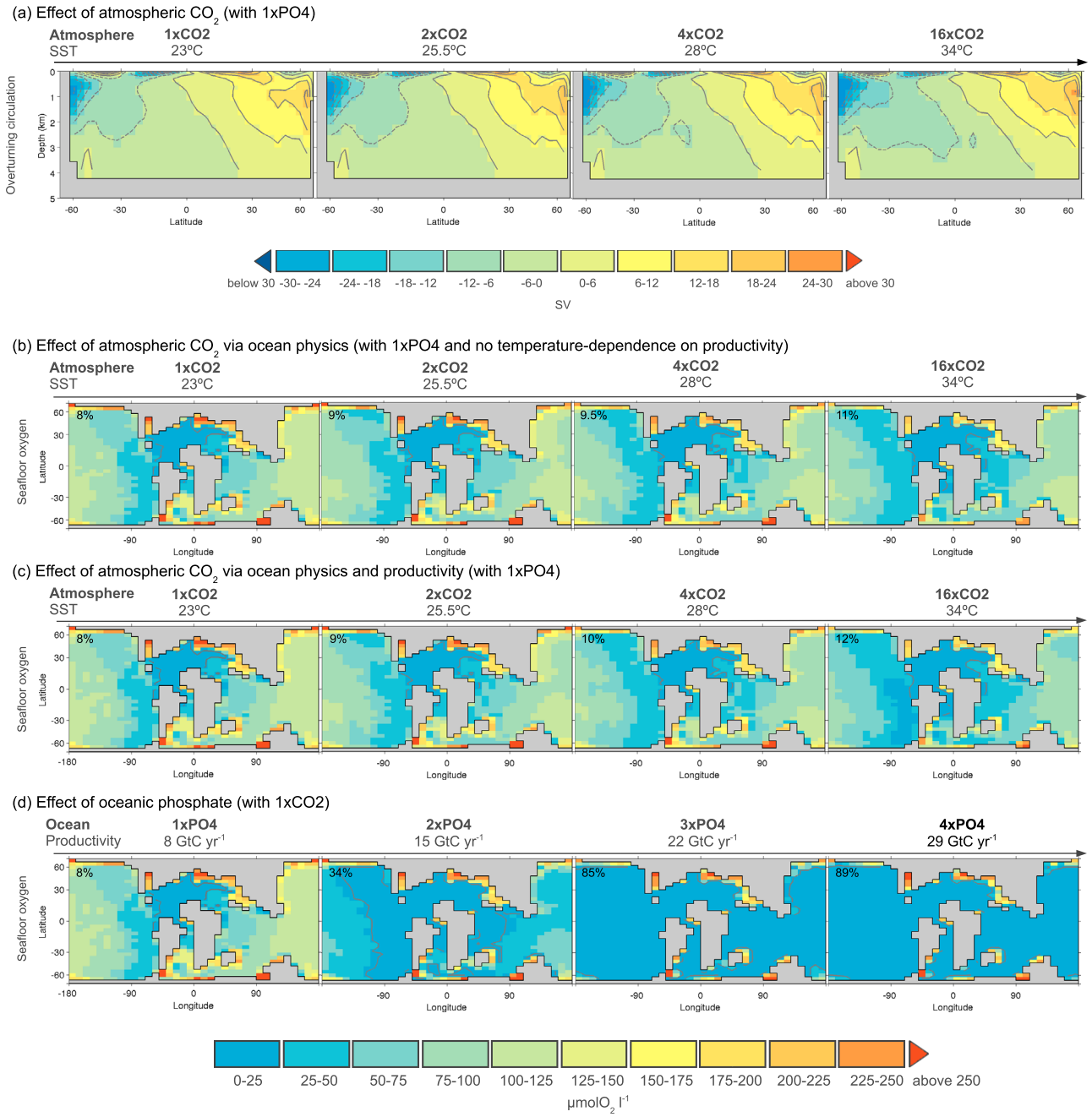


**Figure 3.** Model sensitivity of ocean circulation and seafloor oxygen with changing atmospheric $CO_2$ and oceanic phosphate (SENSITIVITY and NOBIOTEMP experiments). Annual mean sea-surface temperatures (SST) are indicated for the $CO_2$ sensitivity experiments, and export production for the $PO_4^{-3}$ sensitivity experiment. (a) Global meridional overturning circulation; (b–d) Model oxygen concentration at the seafloor. Gray contour indicates the model oxygen concentration of 10 $\mu$mol $O_2$ $l^{-1}$, delimiting the region of seafloor dysoxia/anoxia. The percentage of the area of seafloor dysoxia/anoxia is indicated on top of each plot. Warming temperature via higher $pCO_2$ does not bring about a significant change in ocean anoxia due to its small effect on oxygen solubility and ocean circulation, whereas enhanced marine productivity via higher phosphate can very quickly drive the seafloor to be anoxic.

[27] The impact of higher nutrient concentration in the ocean is illustrated in Figure 3d from the SENSITIVITY experiments while keeping atmospheric $CO_2$ constant (1 × CO2). There, increasing total oceanic phosphate concentration from modern values to 4 × PO4 enhances global export production from 8 to 29 GtC $yr^{-1}$. As a result, the globally averaged ocean oxygen concentration drops by about 85% (from 110 to 15 $\mu$mol $O_2$ $l^{-1}$), and anoxia spreads across the global ocean with about 90% of the seafloor surface area being dysoxic/anoxic at 4 × PO4. Although only the

(a) Model sensitivity of seafloor dysoxia/anoxia

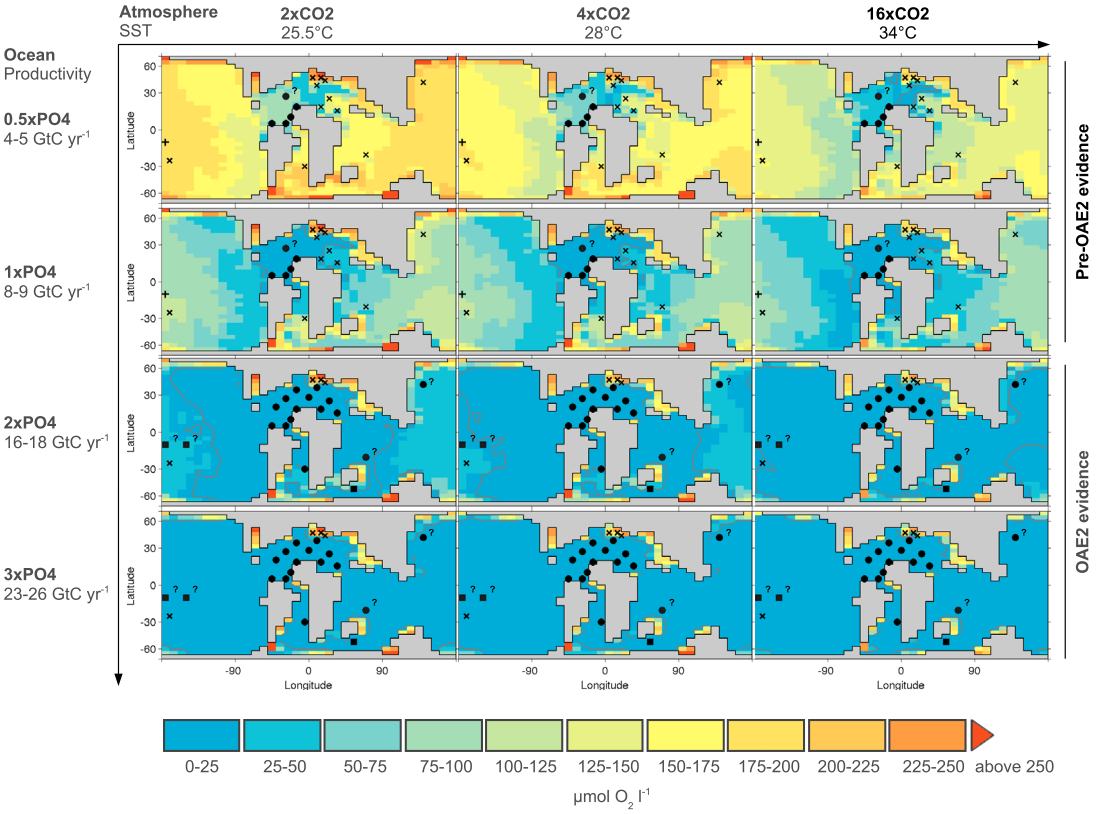


(b) Model sensitivity of photic-zone euxinia

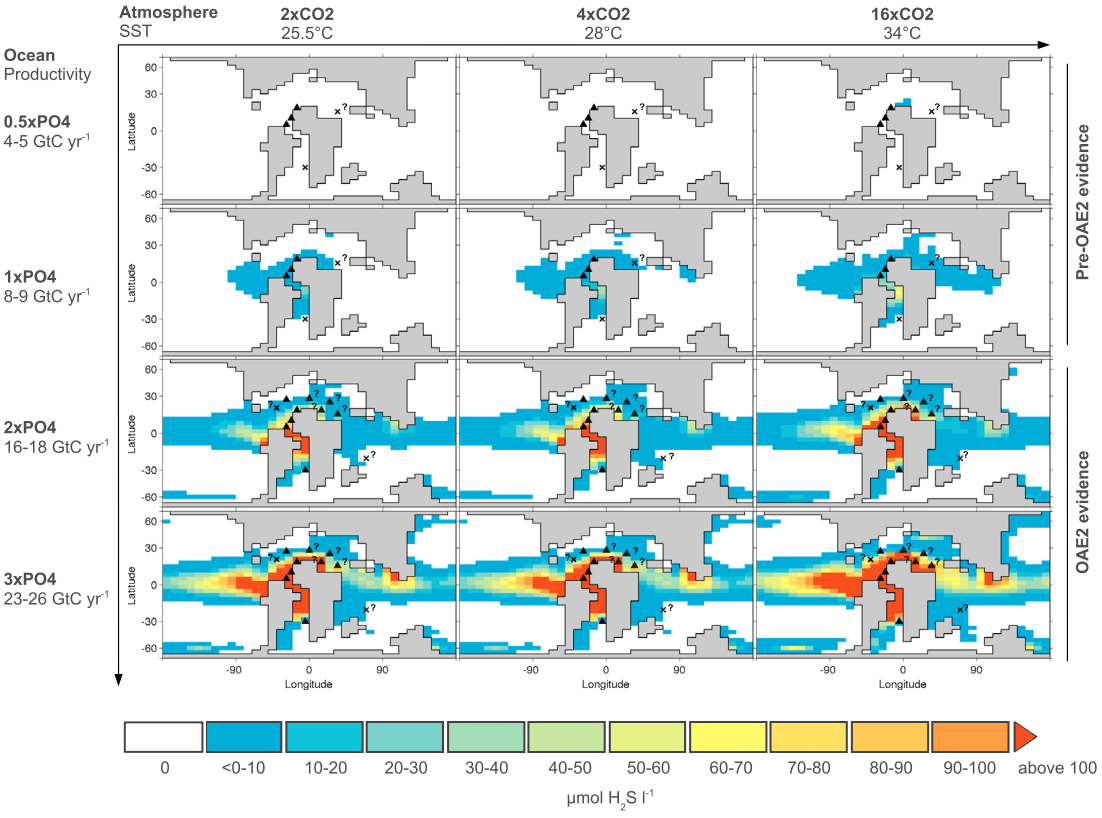


**Figure 4**

**Table 3.** Score for the Model-Data Comparison[a]

| Ocean | Atmosphere | | | Compared data |
|---|---|---|---|---|
| | 2 × CO2 | 4 × CO2 | 16 × CO2 | |
| 0.5 × PO4 | 0.5 | 0.5 | 0.5 | Pre-OAE2 |
| 1 × PO4 | **[0.9]** | **0.9** | **0.9** | |
| 2 × PO4 | 0.7 | 0.7 | 0.6 | |
| 3 × PO4 | 0.6 | 0.6 | 0.6 | |
| 1 × PO4 | 0.6 | 0.7 | 0.7 | OAE2 |
| 2 × PO4 | 0.8 | **[0.9]** | **1.0** | |
| 3 × PO4 | **0.9** | **0.9** | **0.9** | |
| 4 × PO4 | **0.9** | **0.9** | **0.9** | |

[a]A score of 0.0 indicates no agreement and a score of 1.0 total agreement of the model results with the observations. We calculate the score combining observations of seafloor dysoxia/anoxia and photic zone euxinia (see auxiliary material for individual comparison) and taking into account the uncertainty of the evidence (score with questionable evidence is weighted by 0.5, see auxiliary material for full description). Evidence is compared with model results for a series of atmospheric $CO_2$ (2 × −16 × CO2) and for oceanic phosphate inventory varying between 0.5 × −3 × PO4 for pre-OAE2 and between 1 × −5 × PO4 for OAE2. Scores equal or higher than 0.9 are in bold indicating the good agreement of the model results with the observations. Experiments in bracket represent the minimum reconstructions for pre-OAE2 and OAE2, showing that pre-OAE2 oceanic phosphate was similar to today and doubled (or more) during OAE2. Changes in atmospheric $CO_2$ are not well-constrained because of the low sensitivity of oceanic anoxia and euxinia to $pCO_2$ changes.

concentration of phosphate has changed in the model, fixed nitrogen is directly provided by nitrogen fixation (not shown).

[28] We summarize the influence of these mechanisms by introducing the quantity 'oxygen sensitivity' based on the premise of climate sensitivity. Oxygen sensitivity is defined as the change in the global ocean mean concentration of oxygen as a result of doubling atmospheric $CO_2$ or doubling oceanic phosphate. In our Late Cretaceous model, ocean physics (combining the effect on oxygen solubility and circulation) is about five times as efficient at reducing oxygen as the temperature-regulated marine productivity (−10 versus −2 $\mu$mol $O_2$ $l^{-1}$). Whereas when the nutrient effect is considered, marine productivity has an oxygen sensitivity about six times larger than ocean physics (−60 versus −10 $\mu$mol $O_2$ $l^{-1}$). However, although it might not have directly triggered OAE2 via changes in ocean circulation or oxygen solubility, higher $pCO_2$ could have been the underlying driver of a global ocean phosphate increase via elevated continental weathering [*Leckie et al.*, 2002; *Jenkyns*, 2003; *Adams et al.*, 2010; *Jenkyns*, 2010; *Blättler et al.*, 2011].

### 4.2. Reconstruction of OAE2 Redox Changes and Potential Mechanisms

[29] We compare the SENSITIVITY experiments to our compiled evidence of seafloor dysoxia/anoxia and photic zone euxinia (Figure 4). Pre-OAE2 evidence is plotted on top of the 0.5 × −1 × PO4 simulations, and OAE2 evidence on top of the 2 × −3 × PO4 simulations. We assume that $pCO_2$ must have been similar or higher than 2 × CO2, because atmospheric $CO_2$ of the Cretaceous was higher than today [*Bice et al.*, 2006; *Hay*, 2011]. Our model results suggest that temperature alone did not drive the spread of anoxia observed across OAE2, because increasing modeled $pCO_2$ cannot capture the geographical expansion of seafloor anoxia and photic zone euxinia (Figure 4, 1 × PO4 horizontal panels). Even with the extreme atmospheric value of 16 × CO2, anoxia only starts to invade the proto-South Atlantic seafloor and the equatorial Tethys photic zone. A larger expansion of anoxia requires, and is generally well simulated by, enhanced marine productivity.

[30] To reconstruct pre-OAE2 and OAE2 conditions, we score the model agreement with the observations (Table 3). Calculated for each experiment, the score combines seafloor anoxia/dysoxia and photic zone euxinia evidence as well as takes into account the uncertainty of the evidence (0 indicating no agreement and 1 total agreement with the data; see auxiliary material for description of the scoring method). We assume that the model is in good agreement with the observations for a score ≥0.9. The 1 × PO4 and 2 × −16 × CO2 model simulations capture particularly well the pre-event sedimentary and geochemical characteristics (even when evidence from location A is neglected), while the 2 × −5 × PO4 and 2 × −16 × CO2 simulations capture well the proxy data during OAE2. Changes in atmospheric $CO_2$ are not well-constrained because of the low sensitivity of oceanic anoxia and euxinia to $pCO_2$ changes (as described earlier). Our estimation is also limited for the maximum extent of OAE2 anoxia due to the lack of observations in the Pacific Ocean. Nevertheless our reconstruction suggests that OAE2 was associated with a minimum doubling in ocean phosphate (from 1 × PO4 to ≥2 × PO4) and $pCO_2$ (from 2 × CO2 to ≥4 × CO2, assuming $CO_2$ increased prior to and during the earliest parts of OAE2).

[31] Focusing on the low-end OAE2 reconstruction (Figure 5), the model suggests that about half of the ocean became oxygen-depleted during OAE2, with dysoxia/anoxia expanding from 5% of the global ocean volume before OAE2 to 50% during OAE2 (Table 4). In this minimum scenario, seafloor anoxia covered most of the proto-Atlantic, Indian and East Pacific Oceans and most of the Tethys Sea. The model also indicates that photic zone euxinia was already established prior to the event in the East equatorial Pacific Ocean, a prediction that could be tested by future data investigations. During OAE2, photic zone euxinia appears to have expanded into all the equatorial regions and most of the proto-Atlantic Ocean and Tethys Sea. The

**Figure 4.** Model sensitivity of oceanic redox conditions with changing atmospheric $CO_2$ and oceanic $PO_4^{-3}$ in comparison to observations. Annual mean sea-surface temperatures (SST) are indicated for the $CO_2$ sensitivity experiments, and export production for the $PO_4^{-3}$ sensitivity experiments. Plotted on top of the model results are the observations of pre-OAE2 conditions for 1 × −2 × PO4 model simulations, and of OAE2 onset conditions for 3 × −5 × PO4. (a) Sensitivity for seafloor dysoxia/anoxia showing modeled oxygen concentrations at seafloor. Gray contour indicates the model oxygen concentration of 10 $\mu$mol $O_2$ $l^{-1}$, delimiting the region of seafloor dysoxia/anoxia; (b) Sensitivity for photic zone euxinia showing modeled $H_2S$ concentration of the photic zone (80–200 m). Euxinia is defined in the model by the occurrence of free hydrogen sulfide ($H_2S > 0$, in white). Temperature did not drive alone the oceanic redox changes observed across OAE2, because simulations with increasing $pCO_2$ only are far of capturing the observed geographical extent of seafloor anoxia and photic zone euxinia.

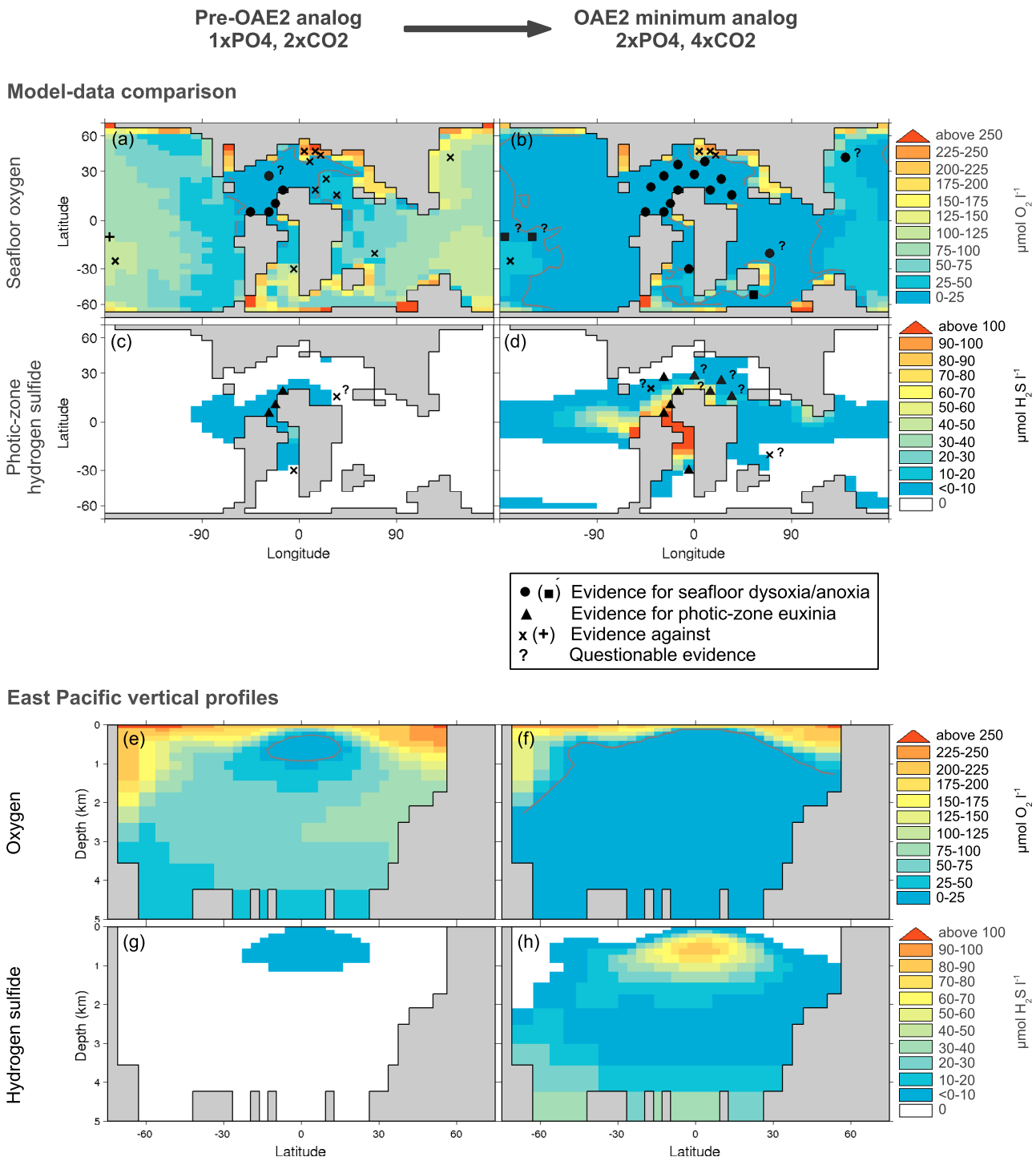


**Figure 5.** Model-data reconstruction of marine biogeochemistry before and during OAE2. (a, b) Seafloor oxygen condition showing modeled oxygen concentration in color. Gray contour indicates the modeled oxygen concentration of 10 $\mu$mol $O_2$ $l^{-1}$, delimiting the region of seafloor dysoxia/anoxia. Black dots and squares indicate evidence for seafloor anoxia/dysoxia, crosses and plus signs indicate evidence against, and question marks indicate the uncertainty of the evidence; (c, d) photic zone free hydrogen sulfide ($H_2S$) condition showing modeled $H_2S$ concentration in color for 80–200 m depth. Euxinia is defined by the occurrence of free hydrogen sulfide ($H_2S > 0$, in white). Black triangles indicate evidence for seafloor anoxia/dysoxia, crosses indicate evidence against, and question marks the uncertainty of the evidence; (e, f) Vertical profile of oxygen in the East Pacific Ocean (−90° longitude); (g, h) Vertical profile of $H_2S$ in the East Pacific Ocean (−90° longitude). We find that the East Pacific Ocean already has photic zone euxinia in the tropics prior to the event, and seafloor anoxia for most parts during OAE2.

**Table 4.** Minimum Changes in Marine Biogeochemistry Across OAE2 From Model Experiments[a]

| Time Period | Atmospheric Carbon Dioxide | Oceanic Mean | | Global Oceanic Dysoxia/Anoxia (Volume %) | Export Production (GtC $yr^{-1}$) |
|---|---|---|---|---|---|
| | | Phosphate | Oxygen ($\mu$mol $O_2$ $l^{-1}$) | | |
| Modern | 1 × CO2 | 1 × PO4 | 150 | 0 | 7 |
| Pre-OAE2 | 2 × CO2 | 1 × PO4 | 100 | 5 | 8 |
| Minimum OAE2 | 4 × CO2 | 2 × PO4 | 30 | 50 | 16 |

[a]Modern values are given as a comparison, with 1 × PO4 equal to 2.15 $\mu$mol P $l^{-1}$ and 1 × CO2 to 278 ppmv (auxiliary material for description of the model experiment). This minimum reconstruction suggests that OAE2 was quasi-global, with at least 50% of the ocean volume to be dysoxic/anoxic.

model-data reconstruction also shows that areas characterized by photic zone euxinia did indeed overlie anoxic intermediate waters (Figures 5e–5h for the East Pacific Ocean) as previously suggested [*Sinninghe Damsté and Köster*, 1998]. Overall, the simulations confirm that OAE2 was a quasi-global event with dysoxia/anoxia spreading to at least 50% of the global ocean volume.

[32] OAE2 is characterized by the model as having a minimum 70% decrease in mean ocean oxygen concentration, from about 100 to 30 $\mu$mol $O_2$ $l^{-1}$ (Table 4). The increase in atmospheric $CO_2$ associated with OAE2 (2 × CO2 to 4 × CO2) results in oceanic oxygen concentrations to drop by about 10 $\mu$mol $O_2$ $l^{-1}$, 15% of the total drop (not shown). This $CO_2$-induced temperature effect arises mainly from the impact of ocean physics, as the temperature impact on marine productivity is responsible for only 5% of the total drop in oxygen. The majority (85%) of the decrease in global oxygen concentrations primarily results in our simulations from enhanced marine productivity via the increase in phosphate concentrations.

[33] Our model-data analysis suggests that OAE2 export production (linked to marine productivity) increased by at least a factor of two (from 8 GtC $yr^{-1}$ to 16 GtC $yr^{-1}$), mainly due to the doubling in phosphate content (and to a second order to warming temperature). While the increase in export production is proportional to the nutrient inventory, oxygen content is not. For a doubling in productivity, the oxygen concentration decreases by a factor of three and dysoxia/anoxia expands by a factor of ten. There is then a non-linear response of the oxygen cycle with changes in marine productivity.

## 5. Discussion

[34] Our minimum estimate suggests that oceanic anoxia during OAE2 was quasi-global covering most of the proto-Atlantic, Indian and Tethys and half of the Pacific seafloor. Even if the Pacific Ocean and East Tethys Sea have very limited data coverage for the Late Cretaceous, our minimum estimate is well constrained especially with respect to evidence from the photic zone. For the model to reproduce photic zone euxinia in most of the proto-Atlantic Ocean and Southwest Tethys Sea as observed at DSDP sites 105/603B and 530A, ODP site 641, in the Apennines and the Levant Platform (Figure 4b), modeled seafloor anoxia has to cover most of the East Pacific basin (Figure 4a). On the other hand, our model-data comparison cannot constrain the maximum extent of OAE2 anoxia. The lack of observations, particularly in the Pacific Ocean, reduced our ability to fully describe the deoxygenation at the Cenomanian-Turonian boundary. More observations would help such as molybdenum isotope evidence of water column euxinia [*Jenkyns*, 2010]. It would be also particularly useful to obtain isorenieratane data at a higher resolution from all sites and any data from the West Pacific Ocean where the boundary between oxic and anoxic conditions occurs in the model. Better $pCO_2$ reconstruction is unlikely to provide better constraints due to the low sensitivity of oceanic anoxia to temperature. However, understanding the mechanisms by which elevated nutrients were provided during the event would provide additional information to determine the change in marine productivity and thus the maximum extent of anoxia at OAE2.

[35] Enhanced marine productivity by nutrients exerts the greatest influence on oceanic redox conditions in our simulations and is likely to be the dominant cause of the widespread OAE2 anoxia. Our model-data reconstruction of OAE2 is consistent with a minimal two-fold increase in marine productivity induced by elevated global oceanic phosphate concentration. Is this OAE2 change in marine productivity due to higher phosphate realistic? Sources of phosphate to the ocean at the Late Cretaceous include continental weathering and phosphorus regeneration [*Jenkyns*, 2010], the latter increasing only after the start of the event as a positive feedback [*Van Cappellen and Ingall*, 1994]. Continental weathering could have started to increase as long as 1 Myrs before OAE2 in association with the enhanced volcanic activity with a final important pulse between 10–20 kyrs before OAE2 [*Turgeon and Creaser*, 2008]. The OAE2 weathering perturbation, therefore, was similar or even longer than the phosphate residence time of the ocean, estimated to be between 10–40 kyrs [*Ruttenberg*, 1993; *Wallmann*, 2003], allowing sources and sinks of phosphorus in the ocean to balance. As a result, a change in phosphate supply to the ocean with OAE2 weathering should have been balanced by a similar change in organic phosphorus burial and an equivalent change in marine production. We expect then that a two-fold increase in marine productivity would have been triggered by a change in continental weathering of similar magnitude (or smaller when phosphorus regeneration is considered). Such a doubling in continental weathering flux can be easily reached within a warming environmental context as suggested by previous modeling studies focusing on other time periods [*Le Hir et al.*, 2009; *Beaulieu et al.*, 2012]. In particular, *Beaulieu et al.* [2012] have shown a high sensitivity for the modern day where a doubling in $CO_2$ results in a 50% increase of the weathering flux over one of the most important Arctic watersheds. Our result is also consistent with the recent study by *Blättler et al.* [2011] which

combined new strontium and calcium isotopic data and estimated a three-fold increase in continental weathering with OAE2.

## 6. Conclusion

[36] We conducted a model-data comparison to reconstruct the redox changes of the global ocean in association with OAE2. Our data set combined indicators of seafloor dysoxia/anoxia and photic zone euxinia before and during the event. These observations were compared with a series of numerical experiments derived from the Earth system model GENIE where we assessed the role of paleogeography, increasing temperature and nutrients on the distribution of oceanic oxygen of the Late Cretaceous. The study led to three important results. First, the predominance of black shales prior to OAE2 in the proto-North Atlantic Ocean might have resulted from the paleogeography of the Late Cretaceous. The proto-North Atlantic Ocean was indeed more inclined to have low oxygen content than the rest of the ocean, because of its silled shape reducing the ventilation of the deep ocean, and the lower latitude of its northern boundary preventing deep-water formation. Second, our model successfully reproduced the observed patterns of oceanic anoxia for before and during OAE2 both at the seafloor and in the photic zone. Our reconstruction suggested that, in addition to the observed pattern, euxinia was already present in the photic zone of the equatorial East Pacific Ocean prior the event and that seafloor anoxia covered most of the proto-North Atlantic Ocean, Tethys Sea and at least half of the Pacific Ocean during OAE2. This minimum OAE2 extent of anoxia in the Pacific Ocean was particularly well constrained and confirmed that OAE2 was quasi-global. Overall oxygen content reduced by at least 70% in the global ocean across OAE2 with global anoxia spreading from 5% to at least 50% of the ocean volume. Finally, our sensitivity analysis showed that enhanced marine productivity by nutrients is much more efficient than ocean physics at removing oxygen from the ocean and was the main mechanism responsible for the widespread anoxia observed during OAE2. We found that oceanic phosphate concentrations would have been similar to those of today prior to OAE2 and could have doubled (or more) during the event, leading to an increase in marine productivity of similar magnitude. While warming might have induced the initial increase in nutrients via weathering, sedimentary anoxia would have maintained elevated oceanic phosphate and productivity via phosphorus regeneration along with nitrogen fixation ensuring sufficient fixed nitrogen. Other OAEs might have also been related to this nutrient-productivity mechanism, as they are associated with warming and potentially weathering increase.

[37] **Acknowledgments.** We thank Christian Bjerrum and Elisabetta Erba for their insightful comments. This research was supported by a Marie Curie Intra-European Fellowship within the 7th European Community Framework Programme (F. M. Monteiro) and a Royal Society University Research Fellowship (A. Ridgwell).

## References

Adams, D. D., M. T. Hurtgen, and B. B. Sageman (2010), Volcanic triggering of a biogeochemical cascade during Oceanic Anoxic Event 2, *Nat. Geosci.*, *3*(3), 201–204, doi:10.1038/ngeo743.

Ando, A., T. Nakano, K. Kaiho, T. Kobayashi, E. Kokado, and B.-K. Khim (2009), Onset of seawater 87Sr/86Sr excursion prior to Cenomanian-Turonian oceanic anoxic event 2? New late Cretaceous strontium isotope curve from the central Pacific Ocean, *J. Foraminiferal Res.*, *39*(4), 322–334.

Arndt, S., A. Hetzel, and H.-J. Brumsack (2009), Evolution of organic matter degradation in Cretaceous black shales inferred from authigenic barite: A reaction-transport model, *Geochim. Cosmochim. Acta*, *73*, 2000–2022, doi:10.1016/j.gca.2009.01.018.

Arthur, M. A., and B. B. Sageman (1994), Marine black shales: Depositional mechanisms and environments of ancient deposits, *Annu. Rev. Earth Planet. Sci.*, *22*, 499–551.

Arthur, M. A., S. O. Schlanger, and H. C. Jenkyns (1987), The Cenomanian-Turonian Oceanic Anoxic Event, II. Palaeoceanographic controls on organic-matter production and preservation, *Spec. Publ. Geol. Soc. London*, *26*(1), 401–420.

Barclay, R. S., J. C. McElwain, and B. B. Sageman (2010), Carbon sequestration activated by a volcanic $CO_2$ pulse during Ocean Anoxic Event 2, *Nat. Geosci.*, *3*(3), 205–208, doi:10.1038/ngeo757.

Beaulieu, E., Y. Goddéris, Y. Donnadieu, D. Labat, and C. Roelandt (2012), High sensitivity of the continental-weathering carbon dioxide sink to future climate change, *Nat. Clim. Change*, *2*(3), 1–4, doi:10.1038/nclimate1419.

Bice, K. L., D. Birgel, P. A. Meyers, K. A. Dahl, K.-U. Hinrichs, and R. D. Norris (2006), A multiple proxy and model study of Cretaceous upper ocean temperatures and atmospheric $CO_2$ concentrations, *Paleoceanography*, *21*, PA2002, doi:10.1029/2005PA001203.

Bjerrum, C. J., J. Bendtsen, and J. J. F. Legarth (2006), Modeling organic carbon burial during sea level rise with reference to the Cretaceous, *Geochem. Geophys. Geosyst.*, *7*, Q05008, doi:10.1029/2005GC001032.

Blättler, C. L., H. C. Jenkyns, L. M. Reynard, and G. M. Henderson (2011), Significant increases in global weathering during Oceanic Anoxic Events 1a and 2 indicated by calcium isotopes, *Earth Planet. Sci. Lett.*, *309*(1–2), 77–88, doi:10.1016/j.epsl.2011.06.029.

Bralower, T. J., and H. R. Thierstein (1984), Low productivity and slow deep-water circulation in mid-Cretaceous oceans, *Geology*, *12*, 614–618, doi:10.1130/0091-7613(1984)12¡614.

Browning, E. L., and D. K. Watkins (2008), Elevated primary productivity of calcareous nannoplankton associated with ocean anoxic event 1b during the Aptian/Albian transition (Early Cretaceous), *Paleoceanography*, *23*, PA2213, doi:10.1029/2007PA001413.

Cao, L., et al. (2009), The role of ocean transport in the uptake of anthropogenic $CO_2$, *Biogeosciences*, *6*(3), 375–390, doi:10.5194/bg-6-375-2009.

Coccioni, R., and V. Luciani (2005), Planktonic foraminifers across the Bonarelli Event (OAE2, latest Cenomanian): The Italian record, *Palaeogeogr., Palaeoclimatol., Palaeoecol.*, *224*, 167–185, doi:10.1016/j.palaeo.2005.03.039.

Courtillot, V. E., and P. R. Renne (2003), On the ages of flood basalt events, *C. R. Geosci.*, *335*(1), 113–140.

Demaison, G. J., and G. T. Moore (1981), Anoxic environments and oil source bed genesis, *Org. Geochem.*, *2*, 9–31.

Donnadieu, Y., R. Pierrehumbert, R. Jacob, and F. Fluteau (2006), Modelling the primary control of paleogeography on Cretaceous climate, *Earth Planet. Sci. Lett.*, *248*, 411–422, doi:10.1016/j.epsl.2006.06.007.

Edwards, N. R., and R. Marsh (2005), Uncertainties due to transport-parameter sensitivity in an efficient 3-D ocean-climate model, *Clim. Dyn.*, *24*, 415–433, doi:10.1007/s00382-004-0508-8.

Eppley, R. W. (1972), Temperature and phytoplankton growth in the sea, *Fish. Bull.*, *70*(4), 1063–1085.

Erba, E. (2004), Calcareous nannofossils and Mesozoic oceanic anoxic events, *Mar. Micropaleontol.*, *52*, 85–106.

Erbacher, J., and J. Thurow (1997), Influence of oceanic anoxic events on the evolution of mid-Cretaceous radiolaria in the North Atlantic and western Tethys, *Mar. Micropaleontol.*, *30*, 139–158.

Erbacher, J., J. Thurow, and R. Littke (1996), Evolution patterns of radiolaria and organic matter variations: A new approach to identify sea-level changes in mid-Cretaceous pelagic environments, *Geology*, *6*, 499–502, doi:10.1130/0091-7613.

Erbacher, J., B. T. Huber, R. D. Norris, and M. Markey (2001), Increased thermohaline strati B. cation as a possible cause for an ocean anoxic event in the Cretaceous period, *Nature*, *409*, 325–327.

Erbacher, J., O. Friedrich, P. A. Wilson, and H. Birch (2005), Stable organic carbon isotope stratigraphy across Oceanic Anoxic Event 2 of Demerara Rise, western tropical Atlantic, *Geochem. Geophys. Geosyst.*, *6*, Q06010, doi:10.1029/2004GC000850.

Fennel, K., M. J. Follows, and P. Falkowski (2005), The co-evolution of the nitrogen, carbon and oxygen cycles in the Proterozoic ocean, *Am. J. Sci.*, *305*, 526–545.

Forster, A., S. Schouten, K. Moriya, P. A. Wilson, and J. S. Sinninghe Damsté (2007), Tropical warming and intermittent cooling during the

Cenomanian/Turonian oceanic anoxic event 2: Sea surface temperature records from the equatorial Atlantic, *Paleoceanography*, *22*, PA1219, doi:10.1029/2006PA001349.

Forster, A., M. M. M. Kuypers, S. C. Turgeon, H.-J. Brumsack, M. Rose, and J. S. Sinninghe Damsté (2008), The Cenomanian/Turonian oceanic anoxic event in the South Atlantic: New insights from a geochemical study of DSDP Site 530A, *Palaeogeogr. Palaeoclimatol. Palaeoecol.*, *267*, 256–283, doi:10.1016/j.palaeo.2008.07.006.

Gale, A. S., A. B. Smith, N. E. A. Monks, J. A. Young, A. Howard, D. S. Wray, and J. M. Huggett (2000), Marine biodiversity through the Late Cenomanian-Early Turonian: Palaeoceanographic controls and sequence stratigraphic biases, *J. Geol. Soc.*, *157*(4), 745–757.

Hague, A. M., D. J. Thomas, M. Huber, R. Korty, S. C. Woodard, and L. B. Jones (2012), Convection of North Pacific deep water during the early Cenozoic, *Geology*, *40*, 527–530, doi:10.1130/G32886.1.

Handoh, I. C., and T. M. Lenton (2003), Periodic mid-Cretaceous oceanic anoxic events linked by oscillations of the phosphorus and oxygen biogeochemical cycles, *Global Biogeochem. Cycles*, *17*(4), 1092, doi:10.1029/2003GB002039.

Handoh, I., G. Bigg, and E. Jones (2003), Evolution of upwelling in the Atlantic Ocean basin, *Palaeogeogr. Palaeoclimatol. Palaeoecol.*, *202*(1–2), 31–58, doi:10.1016/S0031-0182(03)00571-6.

Hardas, P., and J. Mutterlose (2007), Calcareous nannofossil assemblages of Oceanic Anoxic Event 2 in the equatorial Atlantic: Evidence of an eutrophication event, *Mar. Micropaleontol.*, *66*, 52–69, doi:10.1016/j.marmicro.2007.07.007.

Hasegawa, T. (1997), Cenomanian-Turonian carbon isotope events recorded in terrestrial organic matter from northern Japan, *Palaeogeogr. Palaeoclimatol. Palaeoecol.*, *130*(1–4), 251–273, doi:10.1016/S0031-0182(96)00129-0.

Hay, W. W. (2011), Can humans force a return to a Cretaceous climate?, *Sediment. Geol.*, *235*, 5–26, doi:10.1016/j.sedgeo.2010.04.015.

Hetzel, A., M. E. Bottcher, U. G. Wortmann, and H.-J. Brumsack (2009), Paleo-redox conditions during OAE2 reflected in Demerara Rise sediment geochemistry (ODP Leg 207), *Palaeogeogr. Palaeoclimatol. Palaeoecol.*, *273*(3–4), 302–328, doi:10.1016/j.palaeo.2008.11.005.

Higgins, M. B., R. S. Robinson, J. M. Husson, S. J. Carter, and A. Pearson (2012), Dominant eukaryotic export production during ocean anoxic events reflects the importance of recycled $NH_4^+$, *Proc. Natl. Acad. Sci. U. S. A.*, *109*, 2269–2274, doi:10.1073/pnas.1104313109.

Hilbrecht, H., H.-W. Hubberten, and H. Oberhänsli (1992), Biogeography of planktonic foraminifera and regional carbon isotope variations: Productivity and water masses in late Cretaceous Europe, *Palaeogeogr. Palaeoclimatol. Palaeoecol.*, *92*(3–4), 407–421, doi:10.1016/0031-0182(92)90093-K.

Holbourn, A., and W. Kuhnt (2002), Cenomanian-Turonian palaeoceanographic change on the Kerguelen Plateau: A comparison with Northern Hemisphere records, *Cretaceous Res.*, *23*, 333–349, doi:10.1006/cres.2002.1008.

Hunter, S. J., P. J. Valdes, A. M. Haywood, and P. J. Markwick (2008), Modelling Maastrichtian climate: Investigating the role of geography, atmospheric $CO_2$ and vegetation, *Clim. Past Discuss.*, *4*, 981–1019.

Jarvis, I., G. A. Carson, M. K. E. Cooper, M. B. Hart, P. N. Leary, B. A. Tocher, and A. Rosenfeld (1988), Microfossil assemblages and the Cenomanian-Turonian (late Cretaceous) Oceanic Anoxic Event, *Cretaceous Res.*, *9*, 3–103.

Jarvis, I., J. S. Lignum, D. R. Gröcke, H. C. Jenkyns, and M. A. Pearce (2011), Black shale deposition, atmospheric $CO_2$ drawdown, and cooling during the Cenomanian-Turonian Oceanic Anoxic Event, *Paleoceanography*, *26*, PA3201, doi:10.1029/2010PA002081.

Jenkyns, H. C. (2003), Evidence for rapid climate change in the Mesozoic-Palaeogene greenhouse world, *Philos. Trans. R. Soc. London A*, *361*, 1885–1916.

Jenkyns, H. C. (2010), Geochemistry of oceanic anoxic events, *Geochem. Geophys. Geosyst.*, *11*, Q03004, doi:10.1029/2009GC002788.

Jenkyns, H. C., A. Forster, S. Schouten, and J. S. Sinninghe Damsté (2004), High temperatures in the Late Cretaceous Arctic Ocean, *Nature*, *432*, 888–892, doi:10.1038/nature03143.

Jones, C. E., and H. C. Jenkyns (2001), Seawater strontium isotopes, oceanic anoxic events, and seafloor hydrothermal activity in the Jurassic and Cretaceous, *Am. J. Sci.*, *301*, 112–149.

Junium, C. K., and M. A. Arthur (2007), Nitrogen cycling during the Cretaceous, Cenomanian-Turonian Oceanic Anoxic Event II, *Geochem. Geophys. Geosyst.*, *8*, Q03002, doi:10.1029/2006GC001328.

Kaiho, K., and T. Hasegawa (1994), End-Cenomanian benthic foraminiferal extinctions and oceanic dysoxic events in the northwestern Pacific Ocean, *Palaeogeogr. Palaeoclimatol. Palaeoecol.*, *111*, 29–43.

Kolonic, S. (2005), Black shale deposition on the northwest African Shelf during the Cenomanian/Turonian oceanic anoxic event: Climate coupling and global organic carbon burial, *Paleoceanography*, *20*, PA1006, doi:10.1029/2003PA000950.

Kolonic, S., J. S. Sinninghe Damsté, M. E. Bottcher, M. Kuypers, W. Kuhnt, B. Beckmann, G. Scheeder, and T. Wagner (2002), Geochemical characterization of Cenomanian/Turonian Black Shales from the Tarfaya Basin (SW Morocco): Relationships between palaeoenvironmental conditions and early sulphurization of sedimentary organic matter, *J. Pet. Geol.*, *25*(3), 325–350.

Kraal, P., C. P. Slomp, A. Forster, and M. M. M. Kuypers (2010), Phosphorus cycling from the margin to abyssal depths in the proto-Atlantic during oceanic anoxic event 2, *Palaeogeogr. Palaeoclimatol. Palaeoecol.*, *295*, 42–54.

Kuroda, J., and N. Ohkouchi (2006), Implication of spatiotemporal distribution of black shales deposited during the Cretaceous Oceanic Anoxic Event-2, *Paleontol. Res.*, *10*, 345–358.

Kuroda, J., N. Ogawa, M. Tanimizu, M. Coffin, H. Tokuyama, H. Kitazato, and N. Ohkouchi (2007), Contemporaneous massive subaerial volcanism and late cretaceous Oceanic Anoxic Event 2, *Earth Planet Sci. Lett.*, *256*, 211–223, doi:10.1016/j.epsl.2007.01.027.

Kuypers, M. M. M., R. D. Pancost, I. A. Nijenhuis, and J. S. Sinninghe Damsté (2002), Enhanced productivity led to increased organic carbon burial in the euxinic North Atlantic basin during the late Cenomanian oceanic anoxic event, *Paleoceanography*, *17*(4), 1051, doi:10.1029/2000PA000569.

Kuypers, M. M. M., Y. van Breugel, S. Schouten, E. Erba, and J. S. Sinninghe Damsté (2004a), $N_2$-fixing cyanobacteria supplied nutrient N for Cretaceous oceanic anoxic events, *Geology*, *32*(10), 853–856, doi:10.1130/G20458.1.

Kuypers, M. M. M., L. J. Lourens, W. I. C. Rijpstra, R. D. Pancost, I. A. Nijenhuis, and J. S. Sinninghe Damsté (2004b), Orbital forcing of organic carbon burial in the proto-North Atlantic during oceanic anoxic event 2, *Earth Planet Sci. Lett.*, *228*, 465–482.

Le Hir, G., Y. Donnadieu, Y. Goddéris, R. T. Pierrehumbert, G. P. Halverson, M. Macouin, A. Nédélec, and G. Ramstein (2009), The snowball Earth aftermath: Exploring the limits of continental weathering processes, *Earth Planet Sci. Lett.*, *277*(3–4), 453–463, doi:10.1016/j.epsl.2008.11.010.

Leckie, R. M., T. J. Bralower, and R. Cashman (2002), Oceanic anoxic events and plankton evolution: Biotic response to tectonic forcing during the mid-Cretaceous, *Paleoceanography*, *17*(3), 1041, doi:10.1029/2001PA000623.

Li, G., G. Jiang, X. Hu, and X. Wan (2009), New biostratigraphic data from the Cretaceous Bolinxiala Formation in Zanda, southwestern Tibet of China, and their paleogeographic and paleoceanographic implications, *Cretaceous Research*, *30*(4), 1005–1018.

Luciani, V., and M. Cobianchi (1999), The Bonarelli Level and other black shales in the Cenomanian-Turonian of the northeastern Dolomites (Italy): Calcareous nannofossil and foraminiferal data, *Cretaceous Res.*, *20*, 135–167.

Lüning, S., S. Kolonic, E. M. Belhadji, Z. Belhadji, L. Cota, G. Barić, and T. Wagner (2004), Integrated depositional model for the cenomanian-turonian organic-rich strata in north africa, *Earth Sc. Rev.*, *64*, 51–117, doi:10.1016/S0012-8252(03)00039-4.

Meyer, K. M., and L. R. Kump (2008), Oceanic euxinia in Earth history: Causes and consequences, *Annu. Rev. Earth Planet. Sci.*, *36*, 251–288.

Meyers, P. A., S. M. Bernasconi, and J.-G. Yum (2009), Organic Geochemistry 20 My of nitrogen fixation during deposition of mid-Cretaceous black shales on the Demerara Rise, equatorial Atlantic Ocean, *Org. Geochem.*, *40*(2), 158–166, doi:10.1016/j.orggeochem.2008.11.006.

Misumi, K., and Y. Yamanaka (2008), Ocean anoxic events in the mid-Cretaceous simulated by a 3-D biogeochemical general circulation model, *Cretaceous Res.*, *29*(5–6), 893–900.

Monteiro, F. M., S. Dutkiewicz, and M. J. Follows (2011), Biogeographical controls on the marine nitrogen fixers, *Global Biogeochem. Cycles*, *25*, GB2003, doi:10.1029/2010GB003902.

Mort, H. P., T. Adatte, K. B. Föllmi, G. Keller, P. Steinmann, V. Matera, Z. Berner, and D. Stuben (2007), Phosphorus and the roles of productivity and nutrient recycling during oceanic anoxic event 2, *Geology*, *35*(6), 483–486.

Mort, H. P., T. Adatte, G. Keller, D. Bartels, K. Follmi, P. Steinmann, Z. Berner, and E. Chellai (2008), Organic carbon deposition and phosphorus accumulation during Oceanic Anoxic Event 2 in Tarfaya, Morocco, *Cretaceous Res.*, *29*(5–6), 1008–1023, doi:10.1016/j.cretres.2008.05.026.

Murphy, D. P., and D. J. Thomas (2012), Cretaceous deep-water formation in the Indian sector of the Southern Ocean, *Paleoceanography*, *27*, PA1211, doi:10.1029/2011PA002198.

Nederbragt, A. J., and A. Fiorentino (1999), Stratigraphy and palaeoceanography of the Cenomanian-Turonian Boundary Event in Oued Mellegue,

north-western Tunisia, *Cretaceous Res.*, *20*, 47–62, doi:10.1006/cres.1998.0136.

Ohkouchi, N., Y. Kashiyama, J. Kuroda, N. O. Ogawa, and H. Kitazato (2006), The importance of diazotrophic cyanobacteria as primary producers during cretaceous oceanic anoxic event 2, *Biogeosciences*, *3*, 467–478.

Ozaki, K., S. Tajima, and E. Tajika (2011), Conditions required for oceanic anoxia/euxinia: Constraints from a one-dimensional ocean biogeochemical cycle model, *Earth Planet Sci. Lett.*, *304*, 270–279, doi:10.1016/j.epsl.2011.02.011.

Palastanga, V., C. P. Slomp, and C. Heinze (2011), Long-term controls on ocean phosphorus and oxygen in a global biogeochemical model, *Global Biogeochem. Cycles*, *25*, GB3024, doi:10.1029/2010GB003827.

Pancost, R. D., N. Crawford, S. Magness, A. Turner, H. C. Jenkyns, and J. R. Maxwell (2004), Further evidence for the development of photic zone euxinic conditions during Mesozoic oceanic anoxic events, *J. Geol. Soc.*, *161*, 353–364, doi:10.1144/0016764903-059.

Perez-Infante, J., P. Farrimond, and M. Furrer (1996), Global and local controls influencing the deposition of the La Luna Formation (Cenomanian-Campanian), western Venezuela, *Chem. Geol.*, *130*, 271–288.

Poulsen, J. C., E. J. Barron, A. Arthur, and H. Peterson (2001), Response of the mid-Cretaceous global oceanic circulation to tectonic and $CO_2$ forcings, *Paleoceanography*, *16*, 576–592.

Premoli Silva, I., E. Erba, G. Salvini, C. Locatelli, and D. Verga (1999), Biotic changes in cretaceous oceanic anoxic events of the Tethys, *J. Foraminiferal Res.*, *29*, 352–370.

Redfield, A. (1958), The biological control of chemical factors in the environment, *Am. Sci.*, *46*, 205–221.

Ridgwell, A., J. Hargreaves, N. Edwards, J. Annan, T. Lenton, R. Marsh, A. Yool, and A. Watson (2007), Marine geochemical data assimilation in an efficient Earth system model of global biogeochemical cycling, *Biogeosciences*, *4*, 87–104.

Ruttenberg, K. C. (1993), Reassessment of the oceanic residence time of phosphorus, *Chem. Geol.*, *107*(3–4), 405–409, doi:10.1016/0009-2541(93)90220-D.

Sageman, B. B., S. R. Meyers, and M. A. Arthur (2006), Orbital time scale and new C-isotope record for Cenomanian-Turonian boundary stratotype, *Geology*, *34*(2), 125–128, doi:10.1130/G22074.1.

Salvini, G., and M. M. Passerini (1998), The radiolarian assemblages of the Bonarelli Horizon in the Umbria-Marche Apennines and Southern Alps, Italy, *Cretaceous Res.*, *19*, 777–804.

Schlanger, S. O., and H. C. Jenkyns (1976), Cretaceous Oceanic Anoxic Events: Causes and consequences, *Geol. Mijnbouw*, *55*, 179–184.

Schlanger, S. O., M. A. Arthur, H. C. Jenkyns, and P. A. Scholle (1987), The Cenomanian-Turonian Oceanic Anoxic Event, I. Stratigraphy and distribution of organic carbon-rich beds and the marine $\delta_{13}C$ excursion, *Geol. Soc. Spec. Publ.*, *26*, 371–399.

Sepúlveda, J., J. Wendler, A. Leider, H.-J. Kuss, R. E. Summons, and K.-U. Hinrichs (2009), Molecular isotopic evidence of environmental and ecological changes across the Cenomanian-Turonian boundary in the Levant Platform of central Jordan, *Org. Geochem.*, *40*(5), 553–568, doi:10.1016/j.orggeochem.2009.02.009.

Sewall, J. O., R. S. W. van de Wal, K. van der Zwan, C. van Oosterhout, H. A. Dijkstra, and C. R. Scotese (2007), Climate model boundary conditions for four Cretaceous time slices, *Clim. Past*, *3*(4), 647–657, doi:10.5194/cp-3-647-2007.

Sinninghe Damsté, J. S., and J. Köster (1998), A euxinic southern North Atlantic Ocean during the Cenomanian/Turonian oceanic anoxic event, *Earth Planet Sci. Lett.*, *158*, 165–173.

Sinninghe Damsté, J. S., F. Kenig, M. P. Koopmans, J. Koster, S. Schouten, J. M. Hayes, and J. W. de Leeuw (1995), Evidence for gammacerane as an indicator of water column stratification, *Geochim. Cosmochim. Acta*, *59*(9), 1895–1900.

Sinninghe Damsté, J. S., M. M. M. Kuypers, R. D. Pancost, and S. Schouten (2008), The carbon isotopic response of algae, (cyano)bacteria, archaea and higher plants to the late Cenomanian perturbation of the global carbon cycle: Insights from biomarkers in black shales from the Cape Verde Basin (DSDP Site 367), *Org. Geochem.*, *39*(12), 1703–1718, doi:10.1016/j.orggeochem.2008.01.012.

Sinninghe Damsté, J. S., E. C. Van Bentum, G.-J. Reichart, J. Pross, and S. Schouten (2010), A $CO_2$ decrease-driven cooling and increased latitudinal temperature gradient during the mid-Cretaceous Oceanic Anoxic Event 2, *Earth Planet Sci. Lett.*, *293*(1–2), 97–103.

Sliter, W. V. (1995), Cretaceous planktonic foraminifers from sites 865, 866, and 869: A synthesis of Cretaceous pelagic seimentation in the central Pacific Ocean basin, in *Proceedings of the Ocean Drilling Program, Scientific Results*, vol. 143, edited by E. L. Winterer et al., pp. 15–30, College Station, Tex.

Snow, L. J., R. A. Duncan, and T. J. Bralower (2005), Trace element abundances in the Rock Canyon Anticline, Pueblo, Colorado, marine sedimentary section and their relationship to Caribbean plateau construction and oxygen anoxic event 2, *Paleoceanography*, *20*, PA3005, doi:10.1029/2004PA001093.

Summons, R. E., and T. G. Powell (1987), Idenfication of aryl isoprenoids in source rocks and crude oils: Biological markers for the green sulphur bacteria, *Geochim. Cosmochim. Acta*, *51*, 557–566.

Takashima, R., H. Nishi, K. Hayashi, H. Okada, H. Kawahata, T. Yamanaka, A. G. Fernando, and M. Mampuku (2009), Litho-, bio- and chemostratigraphy across the Cenomanian/Turonian boundary (OAE 2) in the Vocontian Basin of southeastern France, *Palaeogeogr. Palaeoclimatol. Palaeoecol.*, *273*, 61–74, doi:10.1016/j.palaeo.2008.12.001.

Takashima, R., H. Nishi, T. Yamanaka, K. Hayashi, A. Waseda, and A. Obuse (2010), High-resolution terrestrial carbon isotope and planktic foraminiferal records of the Upper Cenomanian to the Lower Campanian in the Northwest Pacific, *Earth Planet Sci. Lett.*, *289*(3–4), 570–582, doi:10.1016/j.epsl.2009.11.058.

Trabucho Alexandre, J., E. Tuenter, G. A. Henstra, K. J. van der Zwan, R. S. W. van de Wal, H. A. Dijkstra, and P. L. de Boer (2010), The mid-Cretaceous North Atlantic nutrient trap: Black shales and OAEs, *Paleoceanography*, *25*, PA4201, doi:10.1029/2010PA001925.

Tsandev, I., and C. P. Slomp (2009), Modeling phosphorus cycling and carbon burial during Cretaceous Oceanic Anoxic Events, *Earth Planet. Sci. Lett.*, *286*, 71–79.

Tsikos, H., H. C. Jenkyns, M. R. Petrizzo, A. Forster, S. Kolonic, E. Erba, I. P. Silva, M. Baas, T. Wagner, and J. S. Sinninghe Damsté (2004), Carbon-isotope stratigraphy recorded by the Cenomanian-Turonian Oceanic Anoxic Event: Correlation and implications based on three key localities, *J. Geol. Soc.*, *161*, 711–719, doi:10.1144/0016-764903-077.

Turgeon, S. C., and R. A. Creaser (2008), Cretaceous oceanic anoxic event 2 triggered by a massive magmatic episode, *Nature*, *454*, 323–326, doi:10.1038/nature07076.

Van Cappellen, P., and E. D. Ingall (1994), Benthic phosphorus regeneration, net primary production, and ocean anoxia: A model of the coupled marine biogeochemical cycles of carbon and phosphorus, *Paleoceanography*, *9*(5), 677–692, doi:10.1029/94PA01455.

Voigt, S., A. Gale, and T. Voigt (2006), Sea-level change, carbon cycling and palaeoclimate during the Late Cenomanian of northwest Europe; An integrated palaeoenvironmental analysis, *Cretaceous Res.*, *27*, 836–858, doi:10.1016/j.cretres.2006.04.005.

Voigt, S., A. Aurag, F. Leis, and U. Kaplan (2007), Late Cenomanian to Middle Turonian high-resolution carbon isotope stratigraphy: New data from the Münsterland Cretaceous Basin, Germany, *Earth Planet. Sci. Lett.*, *253*, 196–210, doi:10.1016/j.epsl.2006.10.026.

Wallmann, K. (2003), Feedbacks between oceanic redox states and marine productivity: A model perspective focused on benthic phosphorus cycling, *Global Biogeochem. Cycles*, *17*(3), 1084, doi:10.1029/2002GB001968.

Wan, X., P. B. Wignall, and W. Zhao (2003), The Cenomanian-Turonian extinction and oceanic anoxic event: evidence from southern Tibet, *Palaeogeogr. Palaeoclimatol. Palaeoecol.*, *199*, 283–298.

Wang, C. S., X. M. Hu, L. Jansa, X. Q. Wan, and R. Tao (2001), The Cenomanian-Turonian anoxic event in southern Tibet, *Cretaceous Res.*, *22*, 481–490, doi:10.1006/cres.2001.0271.

Watkins, D. K., M. J. Cooper, and P. A. Wilson (2005), Calcareous nannoplankton response to late Albian oceanic anoxic event 1d in the western North Atlantic, *Paleoceanography*, *20*, PA2010, doi:10.1029/2004PA001097.

Weissert, H., A. Lini, K. B. Föllmi, and O. Kuhn (1998), Correlation of Early Cretaceous carbon isotope stratigraphy and platform drowning events: A possible link?, *Palaeogeogr. Palaeoclimatol. Palaeoecol.*, *137*, 189–203.

Westermann, S., M. Caron, N. Fiet, D. Fleitmann, V. Matera, T. Adatte, and K. B. Föllmi (2010), Evidence for oxic conditions during oceanic anoxic event 2 in the northern Tethyan pelagic realm, *Cretaceous Res.*, *31*(5), 500–514, doi:10.1016/j.cretres.2010.07.001.

Wignall, P. B., and R. Newton (1998), Pyrite framboid diameter as a measure of oxygen deficiency in ancient mudrocks, *Am. J. Sci.*, *298*, 537–552.

Wilson, P. A., and R. D. Norris (2001), Warm tropical ocean surface and global anoxia during the mid-Cretaceous period, *Nature*, *412*, 425–429.